UNIVERSITY OF CALIFORNIA, SAN DIEGO

Understanding the impact of L1 activity in Rett Syndrome using an iPSC-derived 3D model

A Thesis submitted in partial satisfaction of the requirements for the degree
Master of Science

in

Biology

by

Nicole Ashley Suarez

Committee in Charge:

Professor Alysson Muotri, Chair
Professor Terrence Sejnowski, Co-Chair
Professor Brenda Bloodgood

2018

The Thesis of Nicole Ashley Suarez is approved, and it is acceptable in quality and form for publication on microfilm and electronically:

_____

_____
Co-Chair

_____
Chair

University of California, San Diego

2018

DEDICATION

I dedicate this thesis to my parents and my brother, Christian. Thank you for all the sacrifices you have made to allow me the opportunity to receive an education. I love you all.

TABLE OF CONTENTS

LIST OF ABBREVIATIONS

3D: 3-dimensional

3TC: lamivudine, a nucleoside analog reverse-transcriptase inhibitor

APOBEC-3: apolipoprotein B mRNA editing enzyme catalytic polypeptide 3

ASD: autism spectrum disorder

BDNF: brain-derived neurotrophic factor

CpG: a region where a cytosine nucleotide is followed by a guanine nucleotide in the 5' to 3' direction

CTRL: control

d4T: stavudine, a nucleoside analog reverse-transcriptase inhibitor

DMSO: dimethyl sulfoxide

DNA: deoxyribonucleic acid

DPBS: Dulbecco's phosphate-buffered saline

EGF: epidermal growth factor

EGFP: enhanced green fluorescent protein

EN: endonuclease

FBS: fetal bovine serum

FGF: fibroblast growth factor

GDNF: glial cell-derived neurotrophic factor

IGF-1: insulin-like growth factor 1

iPSC: induced pluripotent stem cells

KCC2: potassium-chloride cotransporter-2

KO: knockout

LINE-1 or **L1**: long interspersed element-1

LTR: long terminal repeat

MAP2: microtubule associated protein 2

MeCP2: methyl-CpG binding protein 2

M.O.I: multiplicity of infection

mRNA: messenger RNA

NPC: neural progenitor cells

NT3: neurotrophin-3

NVP: nevirapine, a non-nucleoside reverse-transcriptase inhibitor

ORF: open reading frame

ORF1p: ORF1 protein

ORF2p: ORF2 protein

Pen Strep: Penicillin-Streptomycin

piRNA: PIWI-interacting small RNA

qPCR: quantitative polymerase chain reaction

RC-L1: retrotransposition-competent L1

RNA: ribonucleic acid

RNP: ribonucleotide particle

RT: reverse-transcriptase

RTi: reverse-transcriptase inhibitor (referred to as a treatment combining 3TC and d4T)

RTT: Rett syndrome

SYN: synapsin

TE: transposable element

TEX19.1: testis-expressed protein 19.1

TREX1: three prime repair exonuclease 1

TPRT: target-primed reverse transcription

UTR: untranslated region

VGLUT: vesicular glutamate transporter 1

LIST OF FIGURES

ACKNOWLEDGEMENTS

I would like to acknowledge Dr. Alysson R. Muotri for the opportunity to be a part of his innovative and revolutionizing research team. Being a part of the Muotri Lab has been a defining experience in my life that has helped me grow as a scientist and as a person. I thank you Alysson, the post-docs, and the students for your continuous support.

My sincere thanks also go to Dr. Terrence Sejnowski and Dr. Brenda Bloodgood for their time and effort to be on my committee. Your insightful and valuable comments were crucial to my growth as a scientist. With both of you conducting groundbreaking research in your own disciplines, your encouragement and belief in my abilities were what helped me believe in myself.

Lastly, I want to express a heartfelt thank you to Dr. Angela Macia Ortega. Your love, guidance, and support have extended beyond the laboratory and I can truly call you my life mentor and friend.

ABSTRACT OF THE THESIS

Understanding the impact of L1 activity in Rett Syndrome using an iPSC-derived 3D model

by

Nicole Ashley Suarez

Master of Science in Biology

University of California, San Diego, 2018

Professor Alysson R. Muotri, Chair
Professor Terrence Sejnowski, Co-Chair

Long interspersed element-1 (L1) is a retrotransposon that contributes to approximately 17% of the human genome. L1s can self-mobilize by retrotransposition using their reverse transcriptase and integrate in a new region in the genome. Increased L1 activity is associated with Rett Syndrome (RTT), a neurological disorder that arises due to a mutation in the methyl-CpG-binding protein 2 (*MECP2*) gene. Affected individuals develop seizures, microcephaly, and a regression in motor function and developmental skills. MeCP2 is known to represses L1 expression, however when MeCP2 is absent, like in individuals with RTT, L1 retrotransposition increases. To model the role L1 has on RTT neuropathology, we used induced pluripotent stem

cells (iPSCs) to generate human cortical neurons. We show that L1 retrotransposition plays a role in the abnormal neuronal morphology and decreased synaptogenesis seen in RTT. Furthermore, chronic treatment with reverse-transcriptase inhibitors (RTis), known for limiting L1 activity, shows a rescue of these phenotypes. We also utilized iPSCs to generate 3D neurospheres and cortical organoids to better mimic neuronal architecture and investigate L1's role in synaptogenesis. In RTT cells, we report a significant decrease in neural activity that is improved when treated with RTis. Additionally, RTT organoids exhibited a microcephaly-like reduction in size that was rescued with chronic treatment of RTis. Our results demonstrate that L1 plays a role in the altered neuronal phenotypes seen in RTT and is one of many contributors to the pathophysiology of this disorder.

INTRODUCTION

Long interspersed element-1

Long interspersed element-1 (LINE-1 or L1) is a transposable element (TE), also known as a "jumping gene" due to its ability to move, or transpose, within a genome. L1 is considered a retrotransposon because of its ability to "copy and paste" itself throughout a genome, undergoing an RNA intermediate during its amplification process (Moran and Gilbert 2002). L1s are under the category of non-long terminal repeat (LTR) because of its lack of LTR and are known to be active in the human genome (Mills et al. 2007). L1s contribute to approximately 17% of the human genome (Mills et al. 2007) and are the only known active transposons with the necessary enzymatic machinery to mobilize themselves, making them autonomous (Lander et al. 2001). Brouha and colleagues (2003) studied 90 L1s with intact open reading frames (ORFs) and determined that 44% of them were polymorphic across the human population. Through retrotransposition assays, which determined L1's ability to mobilize in cultured cells, the authors discovered six highly active L1s, termed "hot L1s", that were responsible for 84% of the total retrotransposition capability observed. Five full-length L1s are known to be involved in disease-causing insertions (Dombroski et al. 1991; Holmes et al. 1994; Schwahn et al. 1998; Brouha et al. 2002), possibly playing a role in the predisposition to certain disorders. Indeed, Kazazian and colleagues (1988) reported the first L1 insertion in a patient with hemophilia A, but who had no familial history of the disorder. A new exonic L1 insertion was observed in X-linked gene factor VIII (Kazazian et al. 1988), and since then, over 100 cases of human genetic disorders have been reported caused by *de novo* L1 insertions has occurred (Chen et al. 2005; Belancio et al. 2009; Cordaux and Batzer 2009; Kazazian and Moran 2017).

Retrotransposition of active LINE-1

L1s are able to insert themselves into new locations within the human genome through a copy and paste mechanism as previously mentioned. 500,000 L1 copies are present within the genome (Booth et al. 1996; Lander et al. 2001), however 99% of them are unable to move due to 5' truncation, rearrangement, or mutation (Scott et al. 1987; Dombroski et al. 1991; Goodier 2014; Beck et al. 2010). The 80-100 L1s that are mobile are called retrotransposition competent L1s (RC-L1s) (Brouha et al. 2003; Beck et al. 2010), and contain a promoter within its 5' untranslated region (UTR) with sense and antisense activities, a short 3' UTR, and a poly(A) tail (Dombroski et al. 1991; Scott et al. 1987; Speek 2001). L1 contains two open reading frames, ORF1 and ORF2 that will encode ORF1 and ORF2 proteins in the cytoplasm (ORF1p and ORF2p, respectively) (Moran et al. 1996). ORF1 encodes an RNA binding protein with nucleic acid chaperon activity (Hohjoh and Singer 1997b, a; Martin and Bushman 2001; Khazina and Weichenrieder 2009), while ORF2 produces a protein with enzymatic activities, including an apurinic/apyrimidinc (AP)-like endonuclease (EN) (Martin et al. 1995; Feng et al. 1996) and a reverse-transcriptase (RT) domains, which are both necessary for L1 retrotransposition (Mathias et al. 1991). An ORF0 was recently discovered in the human antisense L1 5' UTR and has the ability to enhance L1 activity, possibly contributing to somatic variation (Denli et al. 2015).

To begin retrotransposition, a full-length L1 messenger RNA (mRNA) is generated using the sense internal promoter in the 5' UTR. The RNA is relocated to the cytoplasm where ORF1p and ORF2p are translated (Alisch et al. 2006; Dmitriev et al. 2007) and binds to the mRNA through a process called *cis*-preference (Wei et al. 2001). The binding of the L1-encoded proteins to the L1-encoding mRNA forms a ribonucleoprotein particle (RNP), which is an essential intermediate for the retrotransposition process (Martin 1991; Kulpa and Moran 2005;

Goodier et al. 2007; Doucet et al. 2010). The L1-RNP is imported back into the nucleus and a new L1 copy is integrated through a process called target-primed reverse transcription (TPRT) (Luan et al. 1993; Cost et al. 2002). In TPRT, the EN domain nicks the bottom strand of the deoxyribonucleic acid (DNA) at a degenerate consensus sequence (5'-TTTT/A-3'), exposing a 3' OH (Jurka 1997; Luan et al. 1993; Cost et al. 2002). The exposed 3'OH is used as a primer for the RT domain (Monot et al. 2013) and the L1 mRNA serves as a template (Luan et al. 1993) to generate complementary DNA (cDNA). While TPRT serves as a model for L1 retrotransposition, alternative mechanisms can exist with the possibility of RT activity occurring in the cytoplasm (Telesnitsky and Goff 1997; Garcia Perez and Alarcon-Riquelme 2017; Thomas et al. 2017).

Regulation of LINE-1 retrotransposition

Throughout mammalian evolution, host factors have tried to prevent retrotransposition at different points of the cycle. Methylation can be considered one host factor that inhibits L1 expression. L1 promoters contain a CpG island with the potential to be methylated, resulting in a reduction of expression (Thayer et al. 1993; Bourc'his and Bestor 2004; Coufal et al. 2009). Early embryogenesis is often associated with hypomethylation, which could possibly explain why there is an accumulation of L1 copies during this period (Munoz-Lopez et al. 2011). In fact, the hypomethylation of L1 promoters is also seen as a defining characteristic of mouse and human embryonic stem cells and induced pluripotent stem cells (iPSCs) (Shen et al. 2006; Garcia-Perez et al. 2007; Munoz-Lopez et al. 2011; Wissing et al. 2012).

At the mRNA level, splicing is considered a regulator of L1 mobilization in somatic tissues and cell cultures due to the generation of non-functional L1 transcripts (Perepelitsa-Belancio and Deininger 2003; Belancio et al. 2006; Sokolowski et al. 2017). Additionally, PIWI

proteins can interact with PIWI-interacting small RNAs (piRNAs) to degrade TE RNA. It has been shown that the piRNA pathway is associated with DNA methylation patterns on repeated elements in mice in order to inhibit L1 expression (Aravin et al. 2007; Aravin et al. 2008; Brennecke et al. 2007; Heras et al. 2014; Xiol et al. 2014; Newkirk et al. 2017). The Microprocessor (Drosha-DGCR8), which is required for microRNA biogenesis, has also been suggested to regulate L1 activity by binding to RC-L1 mRNAs and cleaving hairpin structures within the L1 mRNA, thus reducing L1 encoded proteins and retrotransposition. (Heras et al. 2013). Additionally, Ribonuclease L has been shown to degrade L1 RNA produced by the sense and antisense L1 promoters to reduce retrotransposition (Yang and Kazazian 2006; Zhang et al. 2014).

Lastly, at the post-translational level, many host factors have been described to inhibit L1 mobilization. TEX19.1 has been described to directly interact with and stimulate the degradation of L1 ORF1p in mouse embryonic stem cells (MacLennan et al. 2017). A cytidine deaminase enzyme called APOBEC3 was discovered to have the ability to deaminate and edit L1 sequences, thus inhibiting L1 retrotransposition during the generation of a new cDNA strand (Schumann 2007; Wissing et al. 2011; Marchetto et al. 2013; Richardson et al. 2014). Although many host factors have been described, research continues to be conducted to better understand the evolution and mechanisms of these regulators.

LINE-1 impact in the brain

L1 expression and activity has been observed in the human brain (Muotri et al. 2005; Coufal et al. 2009; Baillie et al. 2011; Evrony et al. 2012; Evrony 2015; Upton et al. 2015). A wide variety of models, ranging from post-mortem brain tissue to rat and human neural cells, have provided evidence to an accumulation of L1 insertions in the brain. In 2005, Muotri and

colleagues demonstrated that an engineered human L1 element had the ability to retrotranspose in rat hippocampal NPCs *in vitro* and in the mouse brain *in vivo*. Additionally, in 2009, Coufal et al. used human fetal brain derived NPCs and human embryonic stem cell (hESC)-derived NPCs to demonstrate the ability for the human brain to support L1 retrotransposition. Researchers in this field have extended beyond the healthy human brain and revealed that certain disease-related genetic mutations can increase the susceptibility for L1 retrotransposition. Recently, researchers studying Aicardi-Goutieres Syndrome, which is a severe neuroinflammatory disorder that often arises due to a mutation in the anti-viral DNase three-prime repair exonuclease 1 (TREX1), used human iPSC-derived neural cells to determine that L1 retroelements significantly contributed to intracellular DNA species within cells, resulting in neurotoxicity (Thomas et al. 2017). Additionally, the accumulation of intracellular DNA consequently causes TREX1-deficient astrocytes to increase type I interferon secretion and increase neurotoxicity (Thomas et al. 2017). Another example is in Ataxia-Telangiectasia, a progressive neurodegenerative disease caused by the mutation in *ataxia telangiectasia mutated (ATM)* gene. Researchers observed a striking increase in retrotransposition events in the hippocampus of *ATM* knockout (KO) mice and a twofold increase in ATM-deficient, hESC-derived NPCs (Coufal et al. 2011). Furthermore, the researchers analyzed copy number of endogenous, human specific L1s in hippocampal sections from Ataxia-Telangiectasia patients and observed an increase in ORF2 copy numbers, indicating an increase in L1 retrotransposition. Patients with schizophrenia, a neuropsychiatric disorder often associated with microdeletions in chromosome 22q11.2, have also been shown to be more susceptible to L1 retrotransposition (Guffanti et al. 2016; Bundo et al. 2014). One study observed high L1 copy numbers in postmortem brain tissue from patients with schizophrenia, specifically from neurons from the prefrontal cortex; as well as an increase in L1 copy number in iPSC-

derived neurons from schizophrenic patients with the 22q11.2 deletion when compared to controls (Bundo et al. 2014). Moreover, another study analyzed 36 postmortem brain tissues of individuals with schizophrenia and reported an increase in intragenic novel L1s in the schizophrenia brains, specifically in dorsolateral prefrontal cortex neurons, when compared to controls (Doyle et al. 2017). Researchers observed that many L1 insertions were found in genes responsible for "cell projection" and "postsynaptic membrane" in the affected individuals and not in control (CTRL) (Doyle et al. 2017).

The existing literature provides evidence for L1 activity in the human brain, however, in order to gain a better understanding of its mechanism and role, a human neurodevelopmental model is necessary, thus iPSC technology provides researchers an optimal model to study human disease,

iPSC disease modeling

The ability to reprogram a somatic cell into an embryonic state has only emerged within recent years (Takahashi and Yamanaka 2006; Takahashi et al. 2007), but this new tool has revolutionized the way scientists study disease. Although human embryonic stem cells can successfully differentiate into various cell types (Thomson et al. 1998), proper disease modeling demanded patient-specific cell lines in order to discover patient-specific cures. The development of iPSCs, along with differentiation protocols for different cell types, has given the scientific field the opportunity to produce "diseased" cells. The neuroscience field is one example that has greatly benefitted from the development of iPSCS. iPSCs have allowed for the study of neural networks from patients with a specific neurological disorder, resulting in the establishment of neurological phenotypes, the discovery of disease mechanisms, and possible treatments (Marchetto et al. 2010; Kang et al. 2014).

iPSC technology has proven its revolutionary ability in the neuroscience field through the recent development of organoids. Organoids are complex, self-organized, 3-dimensional (3D) structures that aggregate from pluripotent stem cells. They can form different regions of the brain, terming them cerebral organoids, and can alternatively be generated to resemble a specific brain region. Lancaster and colleagues (2013) generated the first brain-like organoids from iPSCs that developed cortical-like regions paralleling the organization of an early developing human cortex. Organoids offer the benefit of studying a disease in a 3D structure and investigating the progress of a diseased cell line throughout the structure's recapitulation during neural development. Since 2013, organoids have been used as models for numerous neurological disorders including microcephaly (Lancaster et al. 2013), Miller-Dieker syndrome (Bershteyn et al. 2017; Iefremova et al. 2017), autism spectrum disorder (ASD) (Mariani et al. 2015), and Alzheimer disease (Choi et al. 2014). Additionally, organoids have also shown its potential to study viral infections from its use to study the Zika virus infection during the 2016 Zika virus outbreak (Garcez et al. 2016; Cugola et al. 2016). The ability for organoids to self-organize and recapitulate human neurodevelopment make them the ideal model to study human brain development and human neurological disorders. In this project, we utilize iPSC technology to model Rett Syndrome and investigate the contribution L1 activity has on this disorder.

Rett syndrome

Rett syndrome (RTT) is a progressive neurological disorder associated with the mutation of the X-linked gene methyl-CpG binding-protein 2 (MeCP2) (Amir et al. 1999). MeCP2 acts as a transcriptional repressor by binding to methylated CpG dinucletides within promoters to epigenetically regulate its targets (Yasui et al. 2007; Chahrour et al. 2008). RTT is often caused by the X-linked dominant pattern of inheritance. Due to its effect on the X-chromosome,

individuals living with RTT are predominantly female, and a spectrum of phenotypes are noted due to mutant MeCP2 X-inactivation or the severity of the mutation. Hemizygous males have more severe phenotypes and are known to rarely live past birth. Patients with RTT are often considered a part of the ASD population due to their autistic characteristics (Hammer et al. 2002; Samaco et al. 2005; Samaco et al. 2004; Zappella et al. 2003). These individuals follow typical development until 6-18 months of age, when an impairment of motor function, a regression of developmental skills, hypotonia, and seizures occur (Amir et al. 1999). Although there is currently no cure for RTT, many researchers have utilized RTT patient cell lines to better understand the disorder.

Marchetto and colleagues (2010) introduced the first iPSC culture system to model RTT using reprogrammed RTT patients' fibroblasts. The iPSCs were differentiated into neurons and the authors showed a neuronal morphological difference between RTT neurons and controls (CTRL). By measuring glutamatergic neurons through vesicular glutamate transporter 1 (VGLUT1) antibodies, the researchers discovered a reduction in VGLUT1 puncta on microtubule associated protein 2 (MAP2)-labelled RTT neuron dendrites, suggesting a decrease in excitatory synapses. Additionally, by infecting neurons with a lentivirus expressing the *enhanced green fluorescent protein (EGFP)* gene under the control of Synapsin 1 (SYN) (SYN::EGFP), the authors revealed smaller soma sizes and a reduction in the number of spines in RTT neurites. SYN::EGFP-infected RTT neurons also displayed electrophysiological defects when whole-cell recordings were performed. Insulin-like growth factor 1 (IGF-1), which has been previously shown to reverse RTT-like symptoms in mice (Tropea et al. 2009), was administered to RTT neurons and authors observed an increase in glutamatergic synapse number, suggesting a potential drug treatment to correct RTT neuronal phenotypes.

These results show that iPSC-derived neural cells can be used as a tool to study RTT and screen for potential drug treatments through its ability to recapitulate the disorder. However, the underlying cause of RTT is still not completely known. RTT is not solely an inherited disorder and only 1% of RTT cases are caused by inherited mutations, while the remaining 99% of cases are considered to be a spontaneous genetic change (Schollen et al. 2003). A possible contributor to these mutations that have recently been explored is L1 and its ability to retrotranspose in the brain.

LINE-1 and Rett Syndrome

As previously mentioned, MeCP2 binds to methylated CpG dinucleotides within promoters of its target genes and transcriptionally represses them (Yasui et al. 2007; Chahrour et al. 2008). L1 5' UTR sequences are known MeCP2 targets and result in methylation-dependent repression (Yu et al. 2001; Klose et al. 2005; Muotri et al. 2010). In order to demonstrate this regulation, Muotri and colleagues (2010) compared CTRL and MeCP2 KO brains of L1-EGFP transgenic mice. L1-EGFP mice have a human RC-L1 tagged with a reporter cassette and an antisense copy of EGFP disrupted by an intron. Because the RC-L1 and the intron are in the same transcriptional orientation but the reporter cassette is not, the expression marker is only detected when the transcript is reverse transcribed, integrated, and expressed by the heterologous promoter (Moran et al. 1996). The researchers observed an increase in EGFP-positive cells in the MeCP2 KO mice brains when compared to CTRLs, proposing an increase in retrotransposition events in the KO mice. Furthermore, this increase was twofold when researchers analyzed human RTT iPSC-derived NPCs, suggesting an association between the loss of function of MeCP2 and the accumulation of L1 insertions in. Lastly, to support these observations *in vivo*, researchers used postmortem human tissues from RTT patients and CTRLs and analyzed the

amount of L1 retrotransposition in the brain and in the heart. Using quantitative polymerase chain reaction (qPCR), the authors quantified the number of L1 ORF2 sequences. Overall, a higher number of ORF2 sequences were observed in brain tissues from both CTRL and RTT patients when compared to heart tissue. In addition, there was a significant increase in the amount of L1 ORF2 sequences in the brains of RTT patients when compared to their CTRLs.

In this thesis, we show that L1 retrotransposition contributes to the altered morphology and synaptogenesis of 2D, iPSC-derived RTT neurons observed in previous studies, and there we observed a rescue of these phenotypes when cells were chronically treated with reverse-transcriptase inhibitors (RTis). Using iPSC-derived 3D neurospheres and cortical organoids, we discovered a partial rescue of spontaneous neural activity of RTT cells when chronically treated with RTis. Lastly, we observed a microcephaly-like reduction in cortical organoid size in RTT cells, but saw a significant rescue in size when the RTT organoids were chronically treated with RTis. Our data demonstrate that L1 retrotransposition plays a role in the reduction of synaptogenesis in RTT, and it is one of many factors that contribute to the disorder.

MATERIALS AND METHODS

Patient consent

Informed consent was obtained from patients who donated CTRL and RTT fibroblasts. Fibroblasts were collected from dermal biopsies under protocols approved by the University of California, San Diego Institutional Review Board (#141223ZF).

Cell culture, neural differentiation, and conditions

iPSCs were cultured on plates coated with matrigel (Corning, CB40234) and fed daily with mTESR1 (StemCell Technologies, 5850). iPSCs were differentiated into NPCs as described in Marchetto et al. (2010). NPCs were cultured on 10 µg/mL poly-L-ornithine (Sigma-Aldrich, P3655) and 2.5 µg/mL laminin (Life Technologies, 23017015) coated plates and the media was changed every other day with NG medium (DMEM/F12 50/50 1X (Corning Cellgro, 15-090-CV), 1% HEPES (VWR International, 45000-694), 0.5% Penicillin Streptomycin (Pen-Strep) (Life Technologies, 15140163), 1X GlutaMAX (Life Technologies, 35050061), 0.5% N2 NeuroPlex (Gemini Bio-Products, 400163) and 1% Gem21 NeuroPlex (Gemini Bio-Products, 400160)), supplemented with 20 ng/mL human fibroblast growth factor basic (bFGF) (R&D Systems, 414-TE). For differentiation into neurons, the bFGF was withdrawn from the NG media and cells were cultured for 5-8 weeks. For differentiation into neurospheres, NPCs were lifted off from the plate and dissociated using StemPro Accutase (Life Technologies, A1110501), and 3-5 million cells were cultured in suspension on 6-well plates (Genesee, 25-105) while shaking at 95 r.p.m. at 37˚C for 48 hours in NG medium, supplemented with bFGF. The bFGF was withdrawn after 48 hours and the neurospheres were kept in NG medium for two weeks.

iPSC-derived cortical organoids were differentiated using a protocol previously described (Pasca et al. 2015) with slight modifications. iPSCs were cultured, dissociated using a 1:1 Dulbecco's phosphate-buffered saline (DPBS, Fisher Scientific, MT21-031CV) and StemPro

Accutase solution, transferred to 6-well plates, and kept in suspension. Neural induction media consisted of DMEM/F12, 1% Glutamax, 1% N2 Neuroplex, 1% non-essential amino acids (Gibco, 11140-050), 1% Pen-Strep, 1μM of Dorsomorphin (Tocris, 309310), and 10μM SB431542 (SB, Stemgent, 04-0010-10). Neural proliferation media consisted of Neurobasal media (Life Technologies, 21103049), 2% Gem21 Neuroplex, 1% non-essential amino acids, 1% Glutamax, 20 ng/mL epidermal growth factor (EGF, Peprotech, AF-100-15), and 20 ng/mL bFGF. For neuronal maturation, the cells were kept in the same media but the growth factors were withdrawn. Organoid results are combined from four separate batches of differentiation.

The reverse-transcriptase inhibitors were prepared as follows: Lamivudine (3TC, Sigma-Aldrich, L1295) was re-suspended in dimethyl sulfoxide (DMSO, Sigma Aldrich, D2650) and 10 μM of 3TC was used in media. Stavudine (d4T, Sigma-Aldrich, D1413) was re-suspended in water and 1μM of d4T was used in media. Nevirapine (Toronto Research, N391275) was re-suspended in DMSO and 400 nM of nevirapine was used in media. CTRL cells contained a dilution of 10 μM of DMSO.

Immunocytochemistry

For adherent cells, cells were washed with DPBS, fixed in 4% paraformaldehyde (PFA, Core Bio, 19943) for 15 minutes at room temperature, and were permeabilized with a solution of DPBS and 0.1% Triton X-100 (Promega, H5142) for 10 minutes at room temperature. Cells were placed in a blocking solution (DPBS, 10% donkey or goat serum (Fisher Scientific, 50413115, 50413116), and 0.005% Triton X-100) and incubated for 30 minutes at room temperature. Primary and secondary antibodies were diluted in solution containing DPBS, 1% donkey or goat serum, and 0.005% Triton X-100. Cells were incubated with the primary antibody overnight at 4˚C. The next day, cells were washed with DPBS three times for 5 minutes and incubated with

secondary antibodies for 30 minutes at room temperature. Cells were washed again with DPBS two times for 5 minutes and the nuclei were stained using DAPI (VWR International, 80051-386, 1:10,000) for 10 minutes. Finally, the cells were washed once with DPBS for 5 minutes and the coverslips were mounted using Prolong Gold antifade mountant (Life Technologies, P36930) onto glass slides (Fisher Scientific, 1255015).

For cells cultured in suspension, cells were washed with DPBS and placed in a 1.5 mL microcentrifuge tube (Fisher Scientific, 7200210) with 4% PFA overnight at 4˚C. Cortical organoids were washed with DPBS and incubated in 30% sucrose (Sigma-Aldrich, S0389) for 48 hours at 4˚C. The tissue was removed from the sucrose solution, placed with optimal cutting temperature compound (OCT, VWR, 25608-930) within an embedding mold (Fisher Scientific, 50465347), and incubated at -80˚C overnight. Using a cryostat (Leica, CM3050S), the molds containing the organoids were sliced at 10.0 µm and placed onto a glass slide which was left to dry at room temperature for at least 4 hours. The slides were lined with a hydrophobic barrier pen (Vector Laboratories, H-4000). Organoid slides were permeabilized, stained and mounted as explained above.

Primary antibody for immunocytochemistry dilutions was used as follows: anti-Synapsin I (Millipore, AB1543P, 1:500), anti-PSD 95 (Antibodies Inc., 75-028, 1:500), anti-MAP2 (Abcam, ab5392, 1:1000), anti-CTIP2 (Abcam, ab18465, 1:350), anti-MECP2 (Diagenode, C15410052, 1:500), anti-GFP (Abcam, ab13970,1:2000), anti-SOX2 (Cell Signaling Technology, 2748S, 1:400), anti-TBR1 (Abcam, ab31940, 1:300), anti-NeuN (Millipore, MAB377, 1:100). Secondary antibodies conjugated to Alexa Fluor 488, 555, and 647 were diluted 1:1000 (Life Technologies).

Retrotransposition assay

CTRL and RTT NPCs were treated with 10 μM of rock inhibitor (Tocris, 125410) for one hour and then were dissociated using StemPro Accutase. 4-5 million cells were nucleofected using the Rat Neural Stem Cell Nucleofection kit (Lonza, VPG-1005) and program A-33 on the Amaxa Nucleofector (Lonza). Cells were transfected with 10 μg of p99-GFP-LRE3-Cherry, which contains a full-length RC-L1 element (LRE3) tagged with a mEGFP1 retrotransposition indicator cassette (Ostertag et al. 2000) within a pCEP4 expression vector (Invitrogen, V04450) which lacks a CMV promoter, but contains an mCherry cassette instead of the puromycin resistance marker. After the transfection, the cells were plated on 6-well plates coated with Poly-L-ornithine and Laminin, and media was changed daily.

To determine the amount of eGFP-positive cells, cells were analyzed by fluorescence active cell sorting (FACS) 7 days post-transfection. Selected cells were treated with 500nM Trichostatin A (Cell Signaling Technology, 9950S) 16 hours before FACS analysis to determine if L1 retrotransposition events were affected by epigenetic silencing (Coufal et al. 2009; Garcia-Perez et al. 2010). The cells were lifted using StemPro Accutase, centrifuged for 4 minutes at 0.2 rpm, and resuspended in FACS buffer (DPBS, 2.5 mM of ethylenediaminetetraacetic acid (EDTA, Life Technologies, 5892791001), 25 mM of HEPES and 5% fetal bovine serum (FBS, Gemini, 900208). Retrotransposition rate was calculated by normalizing the percentage of eGFP-positive cells by the transfection efficiency, determined by the mCherry reporter and by live cell number count.

Morphological analysis of iPSC-derived neurons

NPCs were transduced with a lentivirus backbone containing a Synapsin 1 (SYN) promoter upstream of an EGFP reporter (Nageshappa et al. 2016). The transduction multiplicity

of infection (M.O.I.) was equal to 2. Cells transduced with a SYN::GFP lentivirus were differentiated into neurons for 5-6 weeks, fixed, and stained with GFP and CTIP2 (refer to **Immunocytochemistry** for protocol). Differentiated neurons were traced using Neurolucida version 2017 (MBF Bioscience, Williston, VT) connected to a Zeiss Axio Imager 2 microscope at a 40X oil objective. Only neurons that were both GFP- and CTIP2-positive were included in this analysis. The morphology of the neurons was quantified using Neurolucida Explorer version 11 (MBF Bioscience, Williston, VT) and the results reflect summed length of all neurites and dendrites per traced neuron.

Sholl analysis was performed using Neurolucida Explorer's sholl analysis option. This analysis specified a center point within the soma and created a grid of concentric rings around it with radii increasing in 10 μm increments. Neuronal complexity was determined by recording the number of intersections within each ring.

Synaptic puncta quantification

5-6-week-old neurons were fixed, and stained for the following markers: SYN1, postsynaptic density protein 95 (PSD-95), and MAP2 (refer to **Immunocytochemistry** for protocol). Using a fluorescence microscope (Z1 Axio Observer Apotome Zeiss), the slides were imaged by compiling Z stack images taken from incremental focus distances. Co-localized SYN1 (presynpatic) and PSD-95 (postsynaptic) were quantified using the compiled Z stack image. Only co-localized puncta that were in proximity of a MAP2-positive neurite were included in this analysis.

Measurement of cortical organoid diameter

30-day-old cortical organoids were imaged on an Evos FL Imagine System (ThermoFisher) using a 4X magnification. The images were uploaded to Image J and the diameter of each organoid was determined by the program's length measurement.

RNA extraction

Cells in suspension were washed with DPBS for 5 minutes and placed in Trizol (Life Technologies, 15596018) in a 1.5 mL microcentrifuge tube and dissociated using a 1mL syringe (Fisher Scientific, 1482330) and a needle (VWR, BD- 305196). 24:1 chloroform: isoamyl solution (Invitrogen, 15593031) was added to the tube, shook by hand for 15 seconds, and left at room temperature for 3 minutes. The tube was centrifuged at 12,000 x g for 15 minutes at 4˚C. The aqueous phase was transferred to a new 1.5 mL microcentrifuge tube and one volume of isopropanol (Sigma Aldrich, I9516) was added. The tube was incubated at -80˚C for 60 minutes and centrifuged at 12,000 x g for 15 minutes at 4˚C. The supernatant was removed and cold 70% ethanol (Sigma Aldrich, E7023) was added to the RNA pellet. The tube was centrifuged at 7,500 x g for 7 minutes at 4˚C and the supernatant was removed. The pellet was centrifuged once more and left to dry at room temperature. The pellet was re-suspended in RNase-free water (Lifetech, 10977023), incubated for 10 minutes at 55˚C, and quantified.

qRT-PCR

To obtain complementary DNA (cDNA), the Qiagen Quantitect Reverse Transcription Kit (205310) protocol was followed on 1µg of the RNA samples. A master mix of the primers and SybrGreen (Qiagen, 330500) was generated and placed in ice and away from light. A 96-well or 384-well plate (BioRad) was kept on ice, and the master mix were added to the wells. The cDNA was diluted (1:4) with water and pipetted into the wells. An adhesive film was

applied and the plate was run on a BioRad CFX machine. PCR conditions were as follows: initial cycle of 95ºC for 32 min, followed by 40 cycles of 15s at 95ºC, 30s at 58ºC, 30s at 72ºC, with a final step of 5s at 57ºC and 5s at 95ºC for the melting curve. The following primers were used: **N-55** FWD: GAATGATTTTGACGAGCTGAGAGA; **N-55** REV: GTCCTCCCGTAGCTCAGAGTAATT; **N-22** FWD: CAAACACCGCATATTCTCACTCA; **N-22** REV: CTTCCTGTGTCCATGTGATCTC; **CTIP2** FWD: CTCCCTTTGGATGCCAGTGTCA; **CTIP2** REV: GGCTCCAGGTAGATGCGGAAG; **MAP2** FWD: CAACGGAGAGCTGACCTCA; **MAP2** REV: CTACAGCCTCAGCAGTGACTA.

Multi-electrode array (MEA)

12-well MEA plates (Axion Biosystems, M768-GL1-30Pt200-5) were coated with poly-L-ornithine and laminin. Depending on size, 4-7 neurospheres or organoids were placed in the center of the MEA well to fully cover the electrodes. Neurospheres were plated in NG media supplemented by 1% FBS. One week after plating, neurospheres were changed to media containing 1:1 NG + 1% FBS in neurobasal. Two weeks after plating, the neurosphere media was changed to only neurobasal and kept in this media for the rest of the recordings. Cortical organoids were plated in neuronal maturation media and kept in this media for the rest of the recordings. Both the neurospheres and organoid media was changed twice a week and recordings were measured one day after the media was changed.

Recordings were performed once a week using a Maestro MEA System and AxIS Software (Axion Biosystems). A band-pass filter with 10 Hz and 2.5 kHz cutoff frequencies were used and a spike detector threshold was set to 5.5 times the standard deviation. For each recording, the plate was left untouched in the Maestro for 3 minutes prior to recording, then 3 minutes of data were recorded. Analysis was performed using Axion Biosystems Neural Metrics

Tool. The criteria to detect an active electrode was set to 5 spikes per minute and criteria to detect a burst electrode was set to 5 bursts per minute.

TUNEL Assay

NPCs were cultured on 96-well plates coated with poly-L-ornithine and laminin. Once confluent, the cells were fixed with 4% PFA, permeabilized with 0.1% Triton X-100 for 15 minutes, and were blocked with 3% bovine serum album (Gemini, 700-110) for 60 minutes. Cells were incubated with primary antibodies of Nestin and TUNEL (Click-iT TUNEL assay kit, Life Technologies, C10247) overnight at 4˚C. The following day, the cells were incubated with secondary antibodies for 30 minutes at room temperature, then with DAPI for 5 minutes at room temperature. The cells were mounted using Prolong Gold Antifade mountant and images were taken and quantified.

Statistical Analysis

Technical replicates were used to determine standard error. N is displayed in each figure legend. Standard spreadsheet software (Microsoft Excel version 15.33) was used to organize data. Error bars for figures are standard error of the mean (S.E.M.) using GraphPad Prism v6 (Graphpad Software Inc. version 6.0e). For *t*-test analysis two-tailed unpaired tests with $\alpha = 0.05$ was used. For multiple comparisons, significance was determined with ANOVA, using Tukey's multiple comparisons test. Grabbs' test with $\alpha = 0.05$ was performed to determine outliers, and significant values were excluded from analysis.

RESULTS

Increased L1 retrotransposition events are detected in iPSC-derived RTT NPCs

The cells used in this thesis project were derived from fibroblasts from a RTT patient with a MECP2 mutation in the Methyl-CpG binding domain within Exon 3. This point-nonsense mutation changed a glutamine to a premature stop codon, which resulted in the truncation of the MECP2 protein (**Fig. 1A-C**).

Existing research has shown an increased susceptibility for L1 activity in iPSC-derived RTT NPCs. In 2010, Muotri and colleagues found higher L1 expression in mouse neural stem cells as well as L1 retrotransposition. In addition, researchers electroporated human iPSC-derived CTRL and RTT NPCs with an L1-LRE3-EGFP reporter. This allowed EGFP expression only after retrotransposition was complete. The authors observed a twofold increase in the number of EGFP-positive cells in RTT NPCs when compared to CTRL, suggesting an increase in L1 retrotransposition in RTT cells. In a similar retrotransposition assay, we generated NPCs from iPSCs (**Fig. 1D**) and used a modified reporter construct (p99-GFP-LRE3-Cherry) to transfect CTRL and RTT NPCs. We quantified L1 retrotransposition events using FACS since GFP was only expressed after retrotransposition was complete and integrated (**Fig. 1E**). We observed a significant increase in the number of EGFP-positive cells in RTT, suggesting our RTT cell line indeed has an increased susceptibility for L1 retrotransposition (**Fig. 1F**).

Altered morphology and synaptogenesis in RTT iPSC-derived 2D neurons is rescued through chronic treatment with reverse-transcriptase inhibitors.

Since it has been shown that iPSC-derived NPCs support high rates of L1 retrotransposition when MeCP2 is mutated (Muotri et al. 2010), we decided to differentiate CTRL and RTT NPCs into neurons as described in Marchetto el al. (2010). This protocol predominantly gives rise to cortical neurons of mid-fetal maturity (Marchetto et al. 2010).

Indeed, the human cortex has previously been shown to be more prone to L1 retrotransposition (Muotri et al. 2010), and Marchetto and colleagues (2010) demonstrated that RTT neurons had fewer synapses, smaller soma size, and altered calcium signaling and electrophysiology, so we sought to investigate neuronal morphology in RTT cortical neurons treated with reverse-transcriptase inhibitors (RTis) in order to better grasp the role L1 plays on this phenotype. The RTis used in this study (3TC and d4T) are anti-HIV-1 drugs, but have been shown to inhibit both HIV and L1 reverse transcription (Jones et al. 2008; Thomas et al. 2017). We additionally used another anti-HIV-1 drug (NVP) as a control because no effect on L1 reverse transcription has been demonstrated with the use of this drug (Dai et al. 2011; Jones et al. 2008).

iPSCs were chronically treated with their respective treatments and differentiated into NPCs. TUNEL assay was performed to measure apoptosis and we confirmed that the chronic treatment was not toxic to the cells (**Supp. Fig. 1A-B**). NPCs were transduced with a SYN::EGFP lentivirus to better visualize the neuron for analysis. Transduced NPCs were differentiated for 5-6 weeks, fixed, and stained for GFP to enhance visualization of the labelled neurons. The neurons were also stained for COUP-TF-interacting protein-2 (CTIP2), a cortical neuronal marker, and only GFP and CTIP2 double positive neurons were traced to ensure a cortical neuron analysis (**Fig. 2A**). Morphometric analysis was performed and showed that RTT neurons had smaller cell body areas, fewer branch points, and decreased dendritic length when compared to CTRL neurons (**Fig. 2B-C, 2E-F,** Tukey's multiple comparisons test, *$p<0.05$, ***$p<0.001$, ****$p<0.0001$). This corroborates the observations made by Marchetto et al. (2010). Analysis of RTi-treated RTT neurons displayed a statistically significant increase in cell body area and number of branch points when compared to RTT, whereas this rescue was not seen in NVP-treated RTT neurons (**Fig. 2B-C, 2E,** Tukey's multiple comparisons test, *$p<0.05$,

***p<0.001, ****p<0.0001). Additionally, although not statistically significant, there is a tendency to increase dendrite length in RTi-treated RTT neurons when compared to RTT, with a mean dendrite length of 744 μm and 408 μm, respectively (**Fig. 2B, 2F**). No differences were observed in the number of dendrites between all the treatments (**Fig. 2D**). In order to assess if the RTis treatment was affecting CTRL cells, we also chronically treated them and performed morphometric analysis. We did not find differences when CTRL cells were treated with RTis, suggesting that these retroviral drugs are only improving RTT phenotypes (**Supp. Fig. 2A-E**). Sholl analysis was used to investigate differences between dendritic complexity among the different conditions (**Fig. 2G-H**). According to our analysis, CTRL neurons are significantly more complex when compared to RTT (**Fig. 2G-H**, Tukey's multiple comparisons test, *p<0.05, **p<0.01, ***p<0.001, ****p<0.0001). Additionally, RTi-treated neurons were more complex when compared to RTT (**Fig. 2H**), not seen in the NVP-treated RTT neurons (**Fig. 2H**).

A decrease in glutamatergic synaptogenesis has previously been described in iPSC-derived RTT neurons (Marchetto et al. 2010). In order to determine if treatment with RTis can rescue synapse formation, iPSC-derived NPCs from CTRL and RTT lines were differentiated into neurons for 5-6 weeks. The cell lines were chronically treated with their respective treatments since the iPSC stage and into the NPC and neuronal stages. The neurons were then stained with neuron-specific marker MAP2, pre-synaptic marker SYN1, and post-synaptic marker PSD95 (**Fig. 2I**). Co-localization of SYN1 and PSD95 on a MAP2 positive neurite was quantified. As expected, the RTT neurons exhibited a significant decrease in co-localized puncta when compared to CTRL neurons (**Fig. 2J**, Tukey's multiple comparisons test, ****p<0.0001), as observed in Marchetto et al. (2010). Additionally, RTi-treated RTT neurons displayed a significant increase in co-localized puncta when compared to RTT, which is not seen in NVP-

treated RTT neurons (**Fig. 2J**, Tukey's multiple comparisons test, ****p<0.0001). In addition, we did not find an increase in co-localized puncta in CTRL cells were treated with RTis (**Supp. Fig. 2F**), attributing RTis for the improvement in synaptogenesis.

Reduction of neural activity in RTT iPSC-derived 3D neurospheres is improved through chronic treatment with RTis.

Due to the rescue seen in morphology and synaptogenesis in a 2D neuronal culture, we decided to pursue a more complex model to study synaptogenesis. We differentiated NPCs into 3D neurospheres as described in Nageshappa et al. (2016) (**Fig. 3A**). The NPCs used to generate neurospheres were chronically treated with their respective treatments since the iPSC stage and continued to be treated throughout the experiment. The neurospheres were kept in suspension for 2 weeks and plated on multi-electrode array (MEA) plates to measure synaptogenesis (**Fig. 3B**). The MEA plates were recorded weekly and analysis of spontaneous neural activity was performed after 4 weeks. The raster plots display time stamps of spikes across multiple channels and show that CTRL neurospheres exhibited higher spontaneous neural activity when compared to RTT neurospheres (**Fig. 3C-D**). This significance is also measured by the number of spikes per second (**Fig. 3E**, Tukey's multiple comparisons test, ***p<0.001). A trend was seen in RTi-treated RTT neurospheres exhibiting a higher number of spikes per second when compared to untreated RTT neurospheres (0.010 Hz and 0.0035 Hz, respectively), although this was not statistically significant (**Fig. 3E**). However, when compared to NVP-treated RTT neurospheres, the number of spikes per second was not increased (**Fig. 3E**). No differences were observed when CTRL cells were treated with RTis (**Supp. Fig. 3**). Together, this data suggests there is a decrease in spontaneous neural activity in RTT when compared to CTRL.

Chronic treatment with RTis partially rescued size reduction and neural activity in RTT iPSC-derived 3D cortical organoids.

3D cortical organoids, differentiated from human iPSCs, allows for a spontaneous, self-assembled structure similar to a human neocortex and a transcriptionally similar profile to a mid-fetal prenatal human brain (Lancaster et al. 2013; Pasca et al. 2015) (**Fig 4B-D**). RTT has often been associated with microcephalic phenotype, in which the brain does not develop properly resulting in a smaller than normal head (Hagberg et al. 1983; Hagberg et al. 1993; Hagberg and Skjeldal 1994; Hagberg et al. 1985), so we further utilized iPSC technology to investigate the cytoarchitectural differences using cortical organoids. Indeed, this 3D model has previously been used to study microcephaly in diseases such as Zika Virus or AGS (Lancaster et al. 2013; Cugola et al. 2016; Thomas et al. 2017). We generated cerebral organoids with a cortical fate starting from iPSCs as described in Thomas et al. (2017). Since the iPSC stage, these organoids were chronically treated with their respective treatments. The three main steps of the organoid protocol are neural induction, neural proliferation, and neuronal maturation (**Fig. 4A**). After 34 days of the differentiation process, when the organoids are mature (Thomas et al. 2017), we detected higher L1 expression in RTT organoids using primers in the 5' and the ORF2 domains of the L1 element (**Supp. Fig. 4**). Additionally, the size of the mature organoids was assessed by measuring the diameter. At this stage, the RTT organoids exhibited a statistically significant reduction in diameter when compared to CTRL organoids, however there was a partial rescue with RTis treatment, which was not seen with NVP (**Fig. 4E-F, Supp. Fig. 5**, Tukey's multiple comparisons test, *$p<0.05$, ***$p<0.001$). No significant changes were observed when treating CTRL cells with RTis (**Supp. Fig. 6**).

Because the organoids produced a more mature structure and more complex neural networks, we plated 30-day-old organoids to plate on MEA plates to investigate differences in neural activity (**Fig. 4G**). MEA recordings were performed weekly and analysis of spontaneous neural activity was performed when the organoids were approximately 54 days old. Similar to the neurospheres analysis, the raster plots show that CTRL organoids displayed higher spontaneous neural activity when compared to RTT organoids (**Fig 4H**). This was also represented by looking at the number of spikes per second, where the mean for CTRL organoids was 0.045 Hz and for RTT organoids was 0.012 Hz, yet this was not statistically significant (**Fig 4H-I**). Corroborating the neurospheres analysis, the same trend was seen where the RTi-treated RTT organoids exhibited a higher number of spikes per second when compared to untreated RTT organoids (0.040 Hz and 0.012 Hz, respectively), but this was not statistically significant (**Fig 4I**). The NVP-treated RTT organoids did not exhibit this same increase and only displayed a mean of 0.010 spikes per second. In combination with the neurospheres and organoids analysis, the data continues to suggest a decrease in spontaneous neural activity in RTT and a possible partial rescue of this activity with RTi treatment.

DISCUSSION

Existing literature has shown morphological alterations in human RTT neurons (Marchetto et al. 2010; Armstrong et al. 1995; Kishi and Macklis 2004). Moreover, RTT neurons have also been associated with altered synaptic activity (Marchetto et al. 2010). An upregulation of neuronal L1 retrotransposition in the absence of MeCP2 in rodents and in the presence of MeCP2 mutations in humans has previously been described (Muotri et al. 2010). Here, we corroborate the previous findings, but we additionally suggest that L1 and its ability to reverse transcribe in the brain might contribute to the differences previously observed. We investigated the impact of this retroelement by controlling L1 retrotransposition in a tissue-specific manner, treating human neural cells with reverse-transcriptase inhibitors, 3TC and d4T. Under our experimental conditions, we observed an improvement in RTT neuronal morphology and spontaneous neural activity when treated with these RTis.

The effect of 3TC and d4T on L1 retrotranposition has previously been tested in human L1 RT expressing *E. coli* (Dai et al. 2011), in HeLa cells (Dai et al. 2011; Jones et al. 2008), and more recently, in human three-prime repair exonuclease 1 (*TREX1*) mutant neural cells (Thomas et al. 2017). It was determined that both of these RTis efficiently inhibited L1 reverse transcription. Additionally, we used treatment with NVP on RTT cells as a control since it has been shown to have no effect on L1 reverse transcription (Dai et al. 2011; Jones et al. 2008). With this promising evidence and its ability to cross the blood brain barrier, we decided to utilize iPSC technology and these antiretroviral drugs to determine L1's role in neuronal RTT phenotypes. The cells were chronically treated with their respective treatments since the iPSC stage and throughout the different stages of differentiation.

In order to determine if the RTis could rescue the altered neuronal morphology previously described, we conducted morphometric analysis on iPSC-derived neurons and

determined that cell body area and neuronal complexity was decreased in RTT-derived neurons. Strikingly, this phenotype was rescued with RTi treatment. Additionally, we quantified co-localized pre-synaptic (SYN1) and post-synaptic (PSD95) markers to represent synapse formation. As expected, the RTT-derived neurons had a lower amount of co-localized synaptic puncta when compared to CTRL neurons, however, we discovered that treatment with RTis increased the number of synaptic puncta, implying a partial rescue in synaptogenesis in RTT.

The generation of iPSC-derived neurons has allowed for the ability to study human neurodevelopment and neurological disorders *in vitro*. The advantage to using iPSC-derived neurons is the model's ability to retain the genetic profile from patients with particular mutations throughout the differentiation process, however these neurons are limited in their maturity state and only reach maturity levels to that of a mid-fetus. With the advent of iPSC-derived 3D structures, we utilized these models to determine if the increase in synaptogenesis seen in a monolayer culture translates to an increase in neural activity of these more mature, complex 3D structures. Both RTT neurospheres and cortical organoids exhibited a significant decrease in spontaneous neural activity when compared to the CTRL. RTT neurospheres and cortical organoids treated with RTis exhibited a trend displaying a higher number of spikes when compared to untreated RTT, although this was not statistically significant. This suggests that L1 retrotransposition possibly plays a role in inhibiting synaptogenesis, but there are other aspects that need to be considered in order to generate a full rescue of neural activity.

Additionally, a common phenotype associated with Rett Syndrome is microcephaly (Hagberg et al. 1983; Hagberg et al. 1993; Hagberg and Skjeldal 1994; Hagberg et al. 1985). It has previously been shown that 3TC and d4T have rescued the microcephaly-like reduction in TREX1-deficient organoids, with the authors attributing the rescue to the drugs' effect on

reducing accumulated ssDNA species and consequently lessening apoptosis during neuronal maturation (Thomas et al. 2017). Here, we also measure the diameter of organoids post-neuronal maturation and also observe a decrease in size when RTT organoids are chronically treated with RTis. The results from our study suggest that the morphologically smaller body areas and dendrite length in RTT neurons could contribute to the smaller 3D structure observed in cortical organoids.

Although RTT has no cure, there have been many drugs that have described partial rescues of phenotypes associated with MeCP2 mutations and RTT. In 2009, Tropea and colleagues observed a partial reversal of RTT-like symptoms, including life span, locomotor function, breathing patterns, heart rate, and brain weight, in a mouse model using IGF1 treatment. Furthermore, Marchetto et al. (2010) described an increase in glutamatergic synapse numbers and MeCP2 protein levels in iPSC-derived RTT neurons when they were treated with IGF1. IGF1 was also seen to rescue neuron-specific potassium-chloride cotransporter-2 (KCC2) expression, which is an MeCP2 target and a regulator of GABA functions in the brain, in RTT neurons (Tang et al. 2016). Tang et al. have also suggested further investigation on KCC2 as a potential drug target to rescue delayed GABA functions and treat RTT. Drug candidates that inhibit protein tyrosine phosphatase PTP1B, which is also an MeCP2 target, has also been another therapeutic target for RTT treatment (Krishnan et al. 2015). Increased levels of PTP1B has been associated in MeCP2 dysfunction RTT models, but treatment with PTP1B inhibitors improved survival in male mice and improved behavior in female heterozygous mice (Krishnan et al. 2015). More recently, Na and colleagues (2017) administered FDA-approved drug, D-cycloserine, to a RTT mice model and rescued presynaptic function. D-cycloserine is an amino acid analog of D-alanine which causes an increase in calcium influx when responding to N-

methyl-D-aspartate (NMDA)-mediated glutamatergic signaling (Sheinin et al. 2001) and is known to enhance efficacy of exposure therapies for maladaptive fear (Na et al. 2017; Ressler et al. 2004; Hofmann et al. 2006; Guastella et al. 2008; Kushner et al. 2007; Wilhelm et al. 2008; Otto et al. 2010). The variety of drugs that improve RTT phenotypes, including the RTis used in this study, demonstrate how complex RTT is and establish that there are many contributors to this disorder. Our data suggests that 3TC and d4T could be a beneficial therapeutic approach, but to see a more impactful treatment, should be used in combination with other drugs exhibited to ameliorate RTT phenotypes.

In summary, we have determined that L1 retrotransposition indeed plays a role in morphological differences in RTT-derived neurons. Furthermore, taking advantage of MEA technology, we have demonstrated a decrease in spontaneous neural activity in a 3D organoid model for Rett Syndrome. L1 retrotransposition's role in synaptogenesis remains to be determined, but our results suggest a partial contribution to neural activity. Ultimately, we hope our study will open the discussion and encourage the investigation of L1 and its role in other neurological disorders.

FIGURES

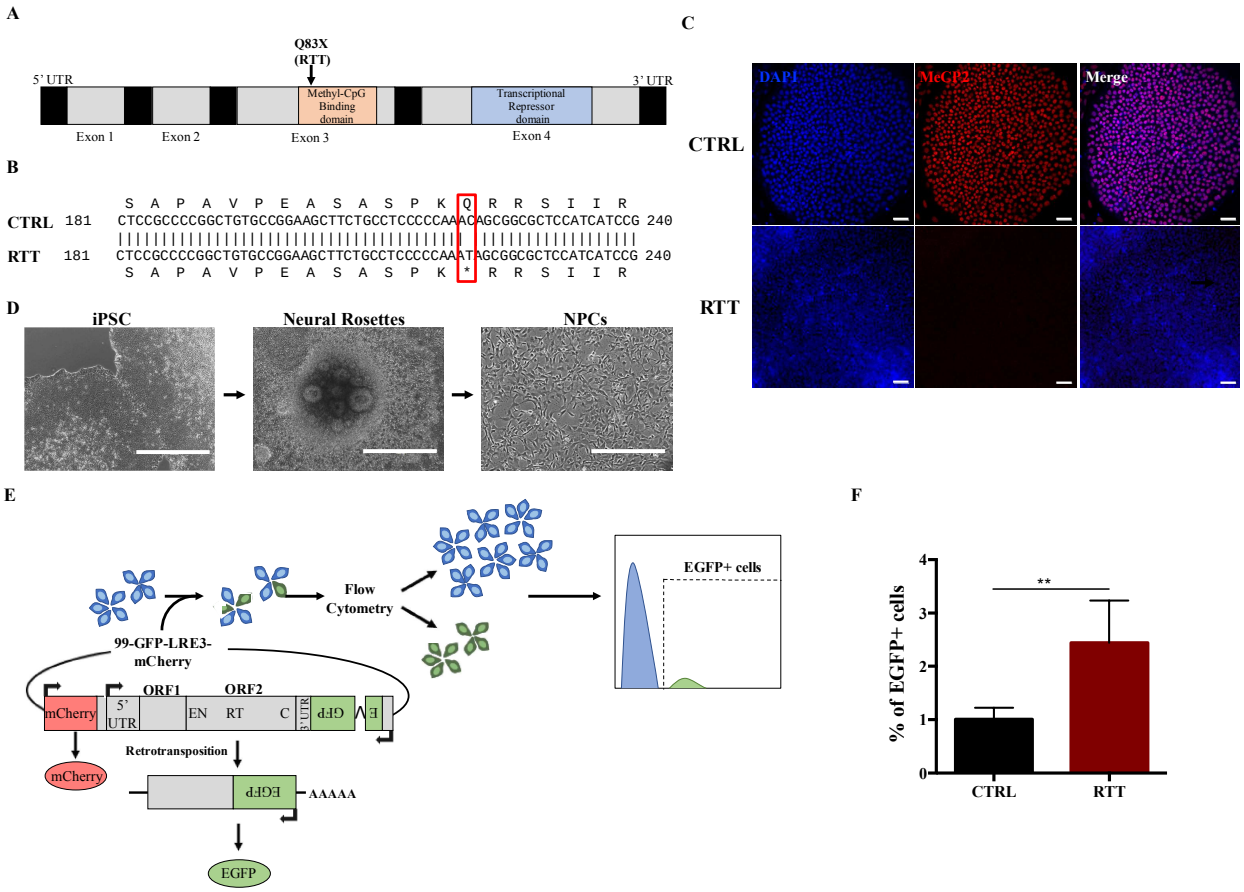

Figure 1. Increased L1 retrotransposition events are detected in iPSC-derived RTT NPCs. **A**. Schematic representation of *MECP2* gene structure and mutation used in this study. **B**. DNA sequence alignment displaying the nucleotide and amino acid change in the *MECP2* sequence in the RTT line. A red box denotes the nucleotide mutation and a * denotes a stop codon. **C**. Representative immunofluorescence images detecting the presence or absence of MeCP2 expression in CTRL (top) or RTT (bottom) induced pluripotent stem cells (iPSCs), respectively. Scale bar, 50 µm. **D**. NPC differentiation protocol. iPSCs were differentiated into neural rosettes. Neural rosettes were isolated and re-plated to obtain NPCs. Scale bar, 1000 µm for iPSCs and neural rosettes; Scale bar, 400 µm for NPCs. **E**. Schematic of retrotransposition assay. NPCs were transfected with 99-GFP-LRE3-mCherry reporter construct and the number of EGFP+ cells were measured using FACS 7 days post-transfection. **F**. Quantification of neural progenitor cells (NPCs) with EGFP-positive cells, which reports the number of de novo retrotransposition events normalized by transfection efficiency and live cell number, **p<0.001, Unpaired t-test.

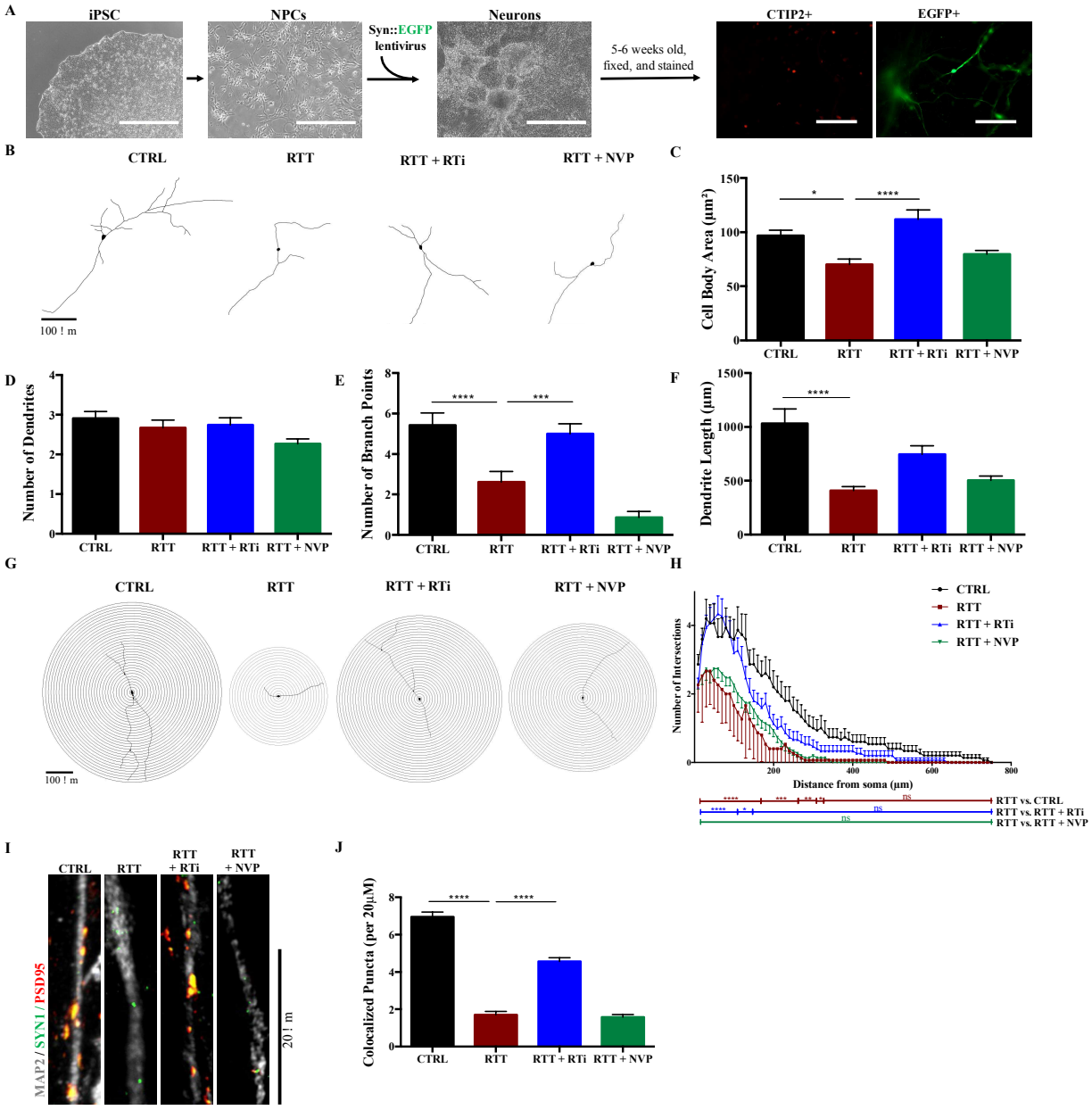

Figure 2. Altered morphology and synaptogenesis in RTT iPSC-derived 2D neurons is rescued through chronic treatment with RTis.

A. Neuronal maturation summary and preparation of neurons for morphometric analysis. iPSCs were differentiated into NPCs. The NPCs were infected with a SYN::EGFP lentivirus and differentiated into neurons for 5-6 weeks. Scale bar, 1000 µm for iPSCs and neurons; Scale bar, 400 µm for NPCs; Scale bar, 100 µm for CTIP+ and EGFP+ neurons. **B**. Representative images of tracings from CTRL, RTT, and RTT treated with RTi or NVP (RTT-treated) neurons. **C-F**. Morphometric analyses of neurons from CTRL, RTT, and RTT-treated. Data are shown as mean ± s.e.m. CTRL, n=22; RTT, n=21; RTT+RTi, n=23; RTT+NVP, n=15. n, number of traced neurons per condition. *p<0.05,***p< 0.001,****p< 0.0001, One-way ANOVA and Tukey's multiple comparisons test. **G**. Representative images of sholl analysis diagrams of neuron

Figure 2. Continued
tracings from the varying conditions. **H**. Sholl analysis of the CTRL, RTT and RTT-treated neurons. n=15. n, number of traced neurons per condition. *p<0.05, **p< 0.01,***p< 0.001,****p< 0.0001, One-way ANOVA and Tukey's multiple comparisons test. **I**. Representative immunofluorescence images of CTRL, RTT, and RTT-treated neuronal dendrites stained for MAP2 (gray), SYN1 (green), and PSD95 (red) from the varying conditions. **J**. Quantification of co-localized synaptic puncta (defined by SYN1+/PSD95+ on MAP2+ dendrite) per 20 μm on neurons from the varying conditions. Data are shown as mean ± s.e.m.,****p< 0.0001, One-way ANOVA and Tukey's multiple comparisons test.

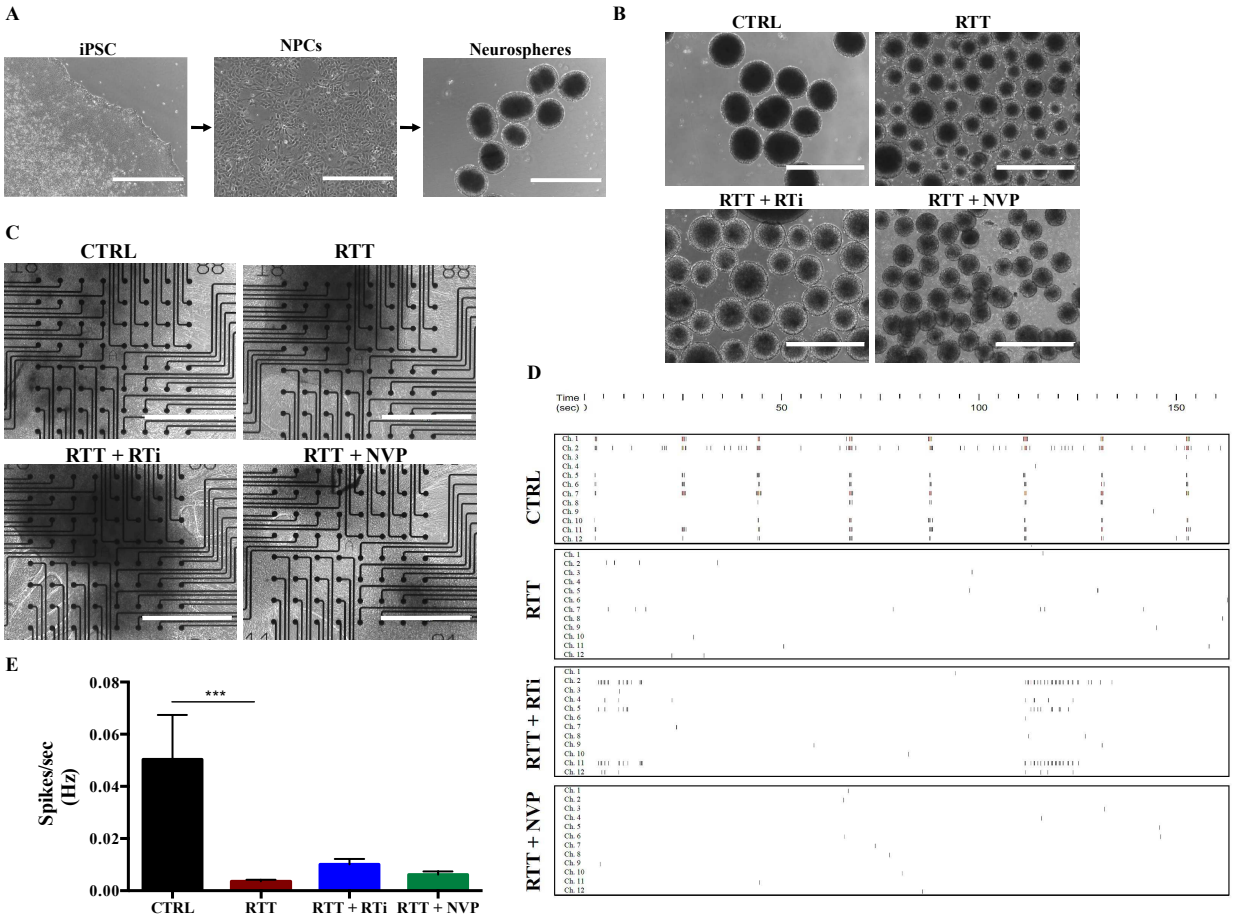

Figure 3. Chronic treatment with RTis improves the altered neural activity in RTT iPSC-derived 3D neurospheres.

A. Neurosphere differentiation protocol. iPSCs were differentiated into NPCs. NPCs were lifted off and kept in rotation on a shaker to generate neurospheres. Scale bar, 1000 µm for iPSCs and neurons; Scale bar, 400 µm for NPCs. **B**. Representative images of day 10 neurospheres derived from CTRL, RTT, and RTT-treated cell lines. Scale bar, 1000 µm. **C**. Representative images of day 40 neurospheres plated on multi-electrode (MEA) plates. Scale bar, 1000 µm. **D**. Raster plots from 40-day-old CTRL, RTT, and RTT with RTi or NVP treatment neurospheres. Representative images of spontaneous activity are shown for a period of 160 seconds for 12 channels. **E**. Number of spikes per second from the varying conditions. Data are shown as mean ± s.e.m. CTRL, n=9; RTT, n=12; RTT+RTi, n=12; RTT+NVP, n=10. n, number of MEA wells measured for each condition. ***p<0.001, One-way ANOVA and Tukey's multiple comparisons test.

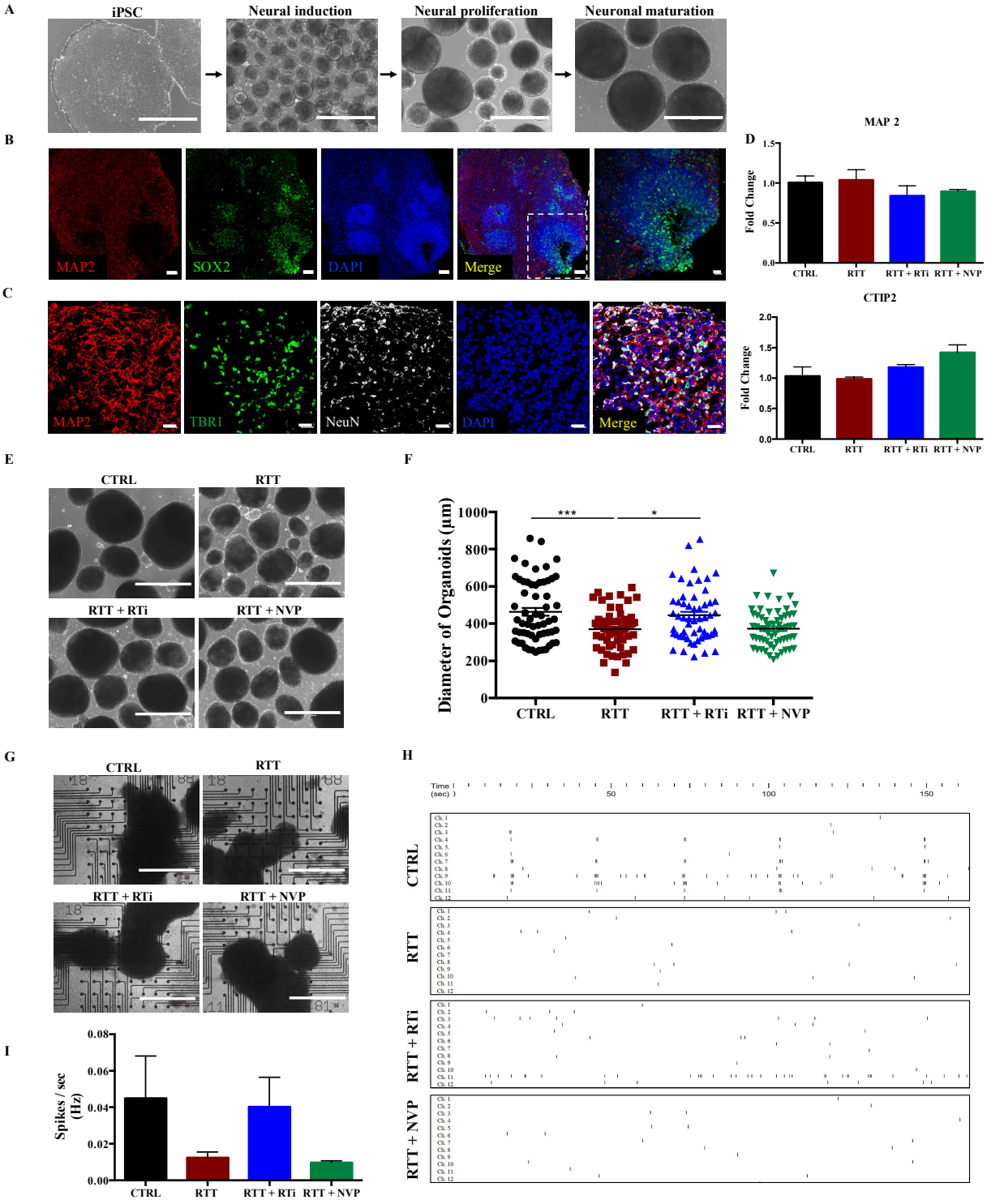

Figure 4. Both size and neural activity in RTT iPSC-derived 3D organoids are partially rescued through chronic treatment with RTis.

A. Cortical organoid differentiation protocol. Starting from iPSCs, the organoid differentiation has three main steps: neural induction, neural proliferation, and neuronal maturation. Scale bar, 1000 µm. **B**. Representative immunofluorescence images of a day 40 CTRL cortical organoid

Figure 4. Continued
stained for MAP2 and SOX2. Scale bar, 50 µm. Scale bar, 20 µm for last panel. **C**. Representative immunofluorescence images of a day 40 CTRL cortical organoid stained for MAP2, TBR1, and NeuN. Scale bar, 20 µm. **D**. Expression of neuronal markers MAP2 and CTIP2 as determined by qPCR. The error bars represent s.e.m. Expression was normalized to the CTRL equaling one. **E**. Representative images of day 34 cortical organoids from the varying treatment conditions used to measure organoid diameter. **F**. Scatterplot showing the quantification of the cortical organoid diameter at day 34 from the varying conditions. The error bars represent s.e.m. CTRL, n=60; RTT, n=60; RTT+RTi, n=55; RTT+NVP, n=60. n, number of cortical organoids measured. *$p<0.05$, ***$p<0.001$. One-way ANOVA and Tukey's multiple comparisons test. **G**. Representative images of day 54 cortical organoids plated on MEA plates. Scale bar, 1000 µm. **H**. Raster plots from 54-day-old CTRL, RTT, and RTT-treated cortical organoids. Representative images of spontaneous activity are shown for a period of 160 seconds for 12 channels. **I**. Number of spikes per second from CTRL, RTT, and RTT-treated organoids. Data is shown as mean ± s.e.m. n=6. n, number of MEA wells measured for each condition.

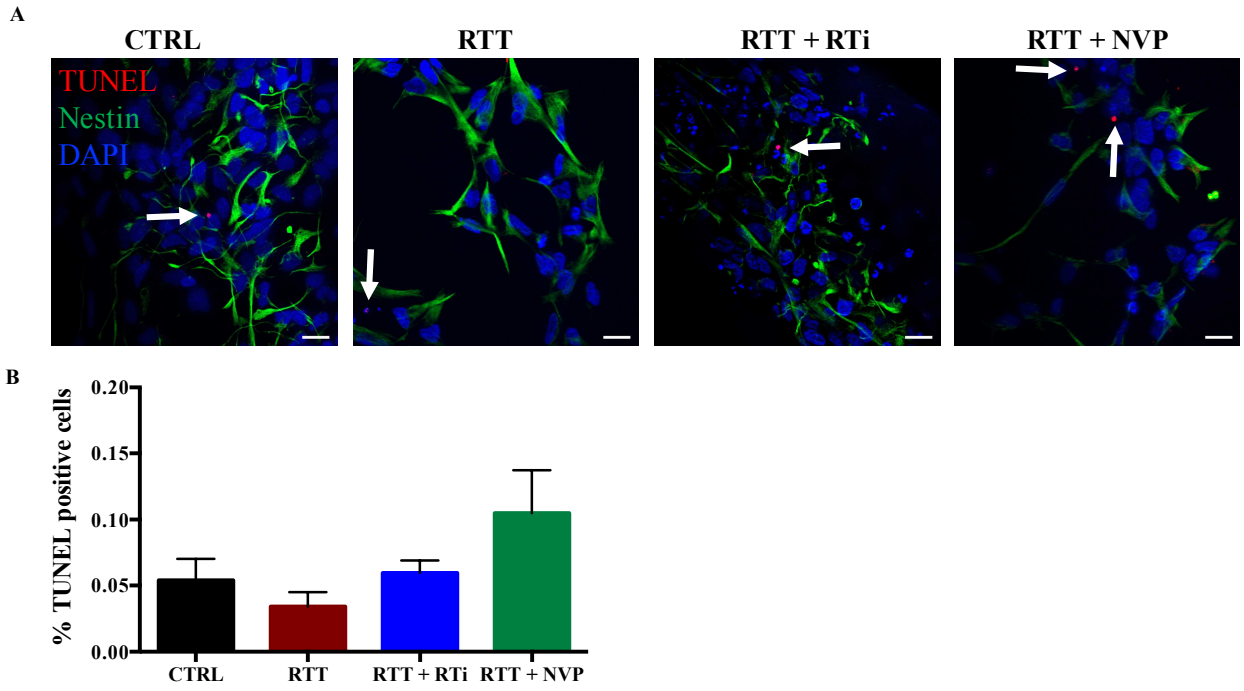

Supplemental Figure 1. RTi treatments are not toxic to iPSC-derived NPCs.
A. TUNEL assay was performed in iPSC-derived NPCs that were chronically treated with RTis. Representative images of immunofluorescence stainings showing TUNEL (red), Nestin (green), and DAPI (blue). White arrows point to TUNEL positive cells. Scale bar, 20 µm. **B**. Quantification of TUNEL positive cells. Data are shown as mean ± s.e.m. One-way ANOVA and Tukey's multiple comparisons test.

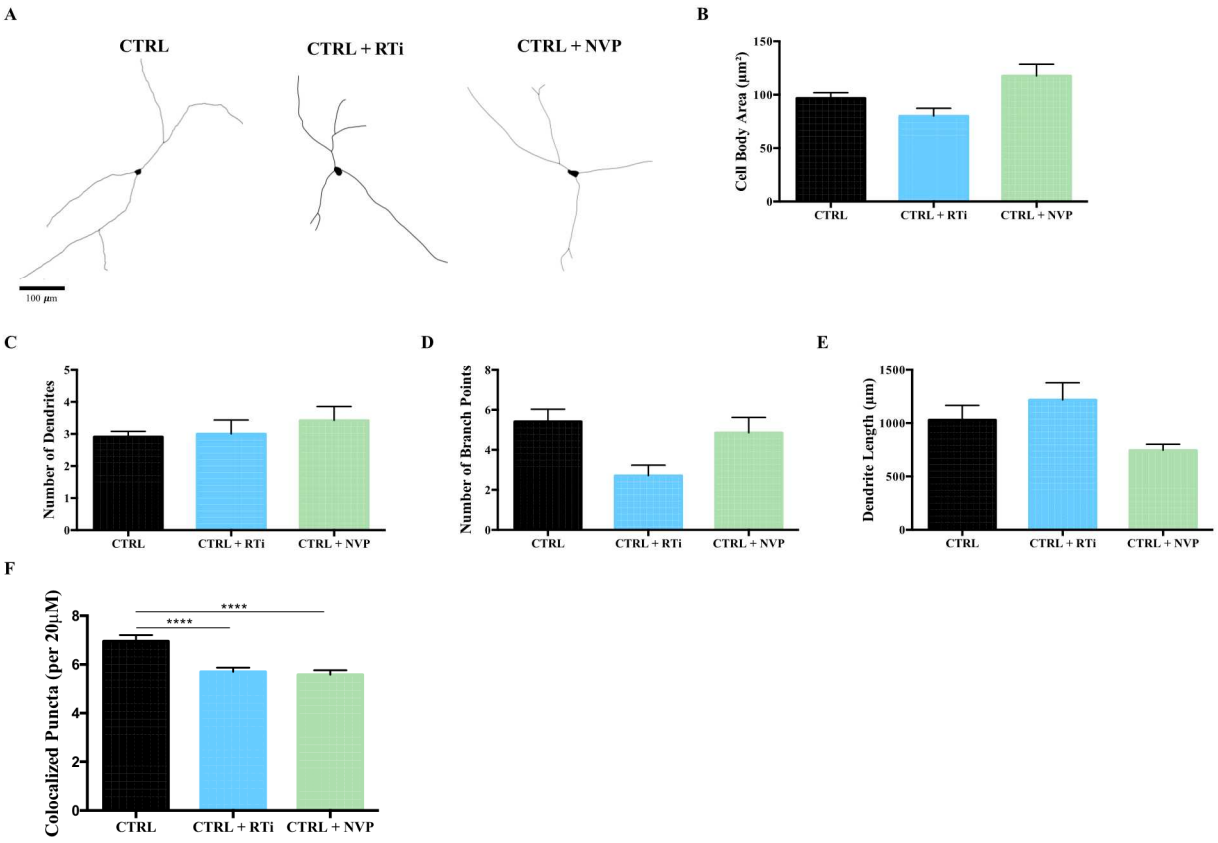

Supplementary Figure 2. Chronic RTi treatment did not affect neuronal morphology in 2D CTRL neurons.

A. Representative tracings of CTRL neurons with their respective treatments.e **B-E**. Morphometric analyses of untreated, RTi-treated, and NVP-treated CTRL neurons. Data are shown as mean ± s.e.m. CTRL, n=22; CTRL + RTi, n=7; CTRL + NVP, n=7. n is number of traced neurons per condition. One-way ANOVA and Tukey's multiple comparisons test. **F**. Quantification of co-localized synaptic puncta per 20 μm of the CTRL and CTRL RTi-treated neurons. Data are shown as mean ± s.e.m. ****p<0.0001, One-way ANOVA and Tukey's multiple comparisons test.

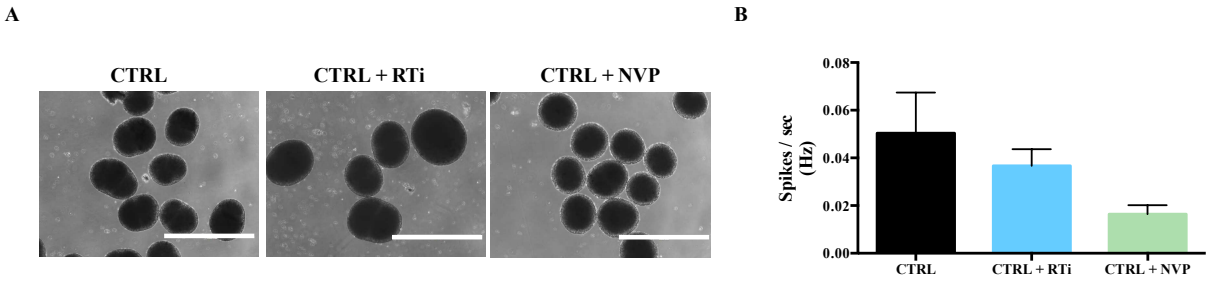

Supplementary Figure 3. Neural activity was not altered in chronically RTi-treated CTRL 3D neurospheres.

A. Representative images of CTRL and CTRL-treated neurospheres at day 10. Scale bar, 1000 µm. **B**. Number of spikes per second from 40-day-old untreated and chronically RTi-treated CTRL neurospheres. Data are shown as mean ± s.e.m. CTRL, n=9; CTRL + RTi, n=7; CTRL + NVP, n=7. n, number of MEA wells measured for each condition. One-way ANOVA and Tukey's multiple comparisons test.

A

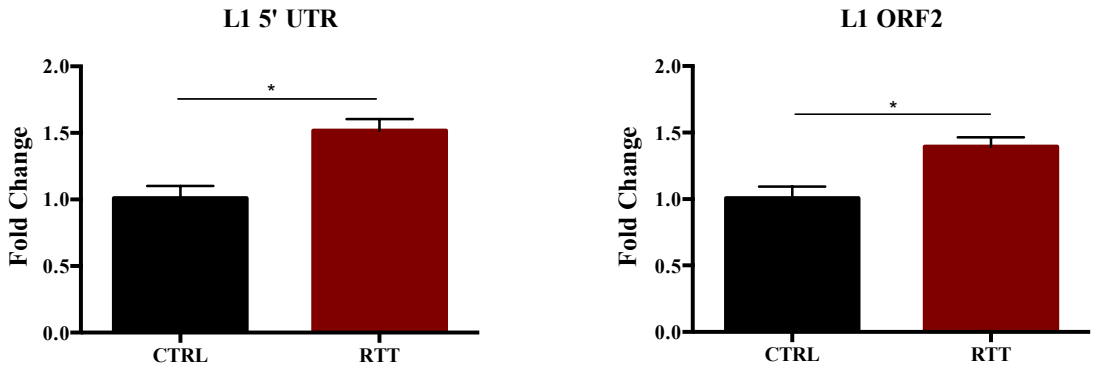

Supplementary Figure 4. L1 elements are higher expressed in RTT iPSC-derived 3D organoids.
L1 expression was analyzed by qRT-PCR using primers in the 5'UTR (left panel) and in the ORF2 domain (right panel) of the active L1 element. Data are shown as mean ± s.e.m. Unpaired*$p<0.016$ (left panel), *$p<0.024$ (right panel), unpaired t-test. n=3, n is number of technical replicates.

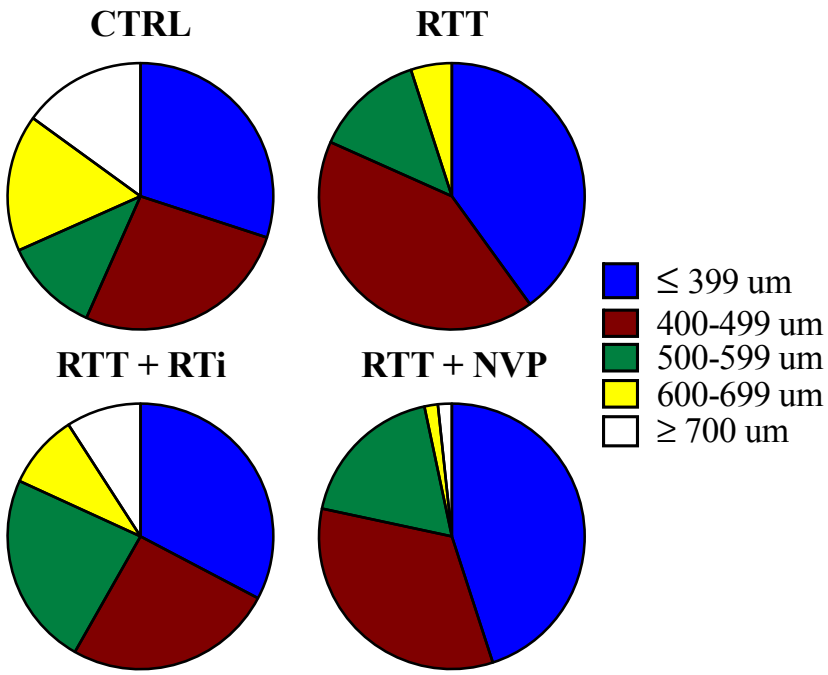

Supplementary Figure 5. Size distribution of diameter of 3D organoids.
Quantification of the diameter of CTRL, RTT, and RTT-treated organoids at day 34 shown as parts of whole pie chart. CTRL, n=60; RTT, n=60; RTT+RTi, n=55; RTT+NVP, n=60. n, number of cortical organoids measured.

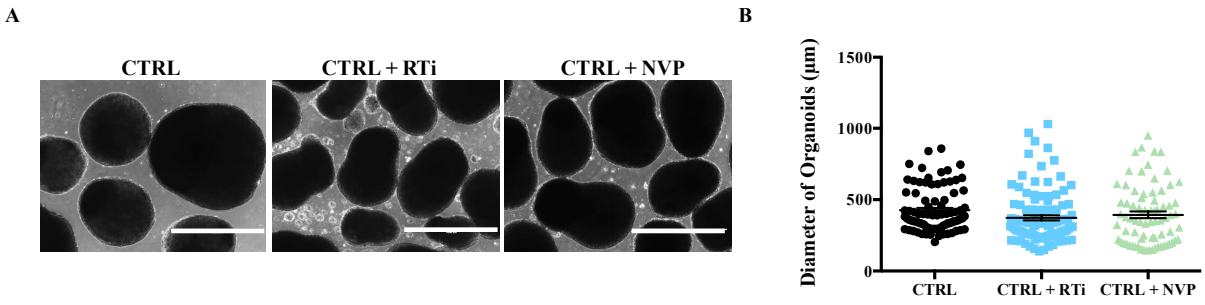

Supplementary Figure 6. CTRL 3D organoids size did not change when treated chronically with RTis.

A. Representative images of 34-day-old CTRL organoids with their respective treatments. Scale bar, 1000 µm. **B**. Quantification of the diameter of organoids shown as a scatterplot. The error bars represent s.e.m. CTRL, n=85; CTRL + RTi, n=108; CTRL + NVP, n=76. n, number of cortical organoids measured. One-way ANOVA and Tukey's multiple comparisons test.

REFERENCES

Alisch RS, Garcia-Perez JL, Muotri AR, Gage FH, Moran JV (2006) Unconventional translation of mammalian LINE-1 retrotransposons. Genes & development 20 (2):210-224. doi:10.1101/gad.1380406

Amir RE, Van den Veyver IB, Wan M, Tran CQ, Francke U, Zoghbi HY (1999) Rett syndrome is caused by mutations in X-linked MECP2, encoding methyl-CpG-binding protein 2. Nature genetics 23 (2):185-188. doi:10.1038/13810

Aravin AA, Hannon GJ, Brennecke J (2007) The Piwi-piRNA pathway provides an adaptive defense in the transposon arms race. Science (New York, NY) 318 (5851):761-764. doi:10.1126/science.1146484

Aravin AA, Sachidanandam R, Bourc'his D, Schaefer C, Pezic D, Toth KF, Bestor T, Hannon GJ (2008) A piRNA pathway primed by individual transposons is linked to de novo DNA methylation in mice. Molecular cell 31 (6):785-799. doi:10.1016/j.molcel.2008.09.003

Armstrong D, Dunn JK, Antalffy B, Trivedi R (1995) Selective dendritic alterations in the cortex of Rett syndrome. Journal of neuropathology and experimental neurology 54 (2):195-201

Baillie JK, Barnett MW, Upton KR, Gerhardt DJ, Richmond TA, De Sapio F, Brennan PM, Rizzu P, Smith S, Fell M, Talbot RT, Gustincich S, Freeman TC, Mattick JS, Hume DA, Heutink P, Carninci P, Jeddeloh JA, Faulkner GJ (2011) Somatic retrotransposition alters the genetic landscape of the human brain. Nature 479 (7374):534-537. doi:10.1038/nature10531

Beck CR, Collier P, Macfarlane C, Malig M, Kidd JM, Eichler EE, Badge RM, Moran JV (2010) LINE-1 retrotransposition activity in human genomes. Cell 141 (7):1159-1170. doi:10.1016/j.cell.2010.05.021

Belancio VP, Deininger PL, Roy-Engel AM (2009) LINE dancing in the human genome: transposable elements and disease. Genome medicine 1 (10):97. doi:10.1186/gm97

Belancio VP, Hedges DJ, Deininger P (2006) LINE-1 RNA splicing and influences on mammalian gene expression. Nucleic acids research 34 (5):1512-1521. doi:10.1093/nar/gkl027

Bershteyn M, Nowakowski TJ, Pollen AA, Di Lullo E, Nene A, Wynshaw-Boris A, Kriegstein AR (2017) Human iPSC-Derived Cerebral Organoids Model Cellular Features of Lissencephaly and Reveal Prolonged Mitosis of Outer Radial Glia. Cell stem cell 20 (4):435-449.e434. doi:10.1016/j.stem.2016.12.007

Booth DR, Ready PD, Smith DF (1996) Evolution of multiple families of non-LTR retrotransposons in phlebotomine sandflies. Genetical research 67 (3):227-237

Bourc'his D, Bestor TH (2004) Meiotic catastrophe and retrotransposon reactivation in male germ cells lacking Dnmt3L. Nature 431 (7004):96-99. doi:10.1038/nature02886

Brennecke J, Aravin AA, Stark A, Dus M, Kellis M, Sachidanandam R, Hannon GJ (2007) Discrete Small RNA-Generating Loci as Master Regulators of Transposon Activity in Drosophila. Cell 128 (6):1089-1103. doi:10.1016/j.cell.2007.01.043

Brouha B, Meischl C, Ostertag E, de Boer M, Zhang Y, Neijens H, Roos D, Kazazian HH, Jr. (2002) Evidence consistent with human L1 retrotransposition in maternal meiosis I. American journal of human genetics 71 (2):327-336. doi:10.1086/341722

Brouha B, Schustak J, Badge RM, Lutz-Prigge S, Farley AH, Moran JV, Kazazian HH, Jr. (2003) Hot L1s account for the bulk of retrotransposition in the human population. Proceedings of the National Academy of Sciences of the United States of America 100 (9):5280-5285. doi:10.1073/pnas.0831042100

Bundo M, Toyoshima M, Okada Y, Akamatsu W, Ueda J, Nemoto-Miyauchi T, Sunaga F, Toritsuka M, Ikawa D, Kakita A, Kato M, Kasai K, Kishimoto T, Nawa H, Okano H, Yoshikawa T, Kato T, Iwamoto K (2014) Increased l1 retrotransposition in the neuronal genome in schizophrenia. Neuron 81 (2):306-313. doi:10.1016/j.neuron.2013.10.053

Chahrour M, Jung SY, Shaw C, Zhou X, Wong ST, Qin J, Zoghbi HY (2008) MeCP2, a key contributor to neurological disease, activates and represses transcription. Science (New York, NY) 320 (5880):1224-1229. doi:10.1126/science.1153252

Chen JM, Stenson PD, Cooper DN, Ferec C (2005) A systematic analysis of LINE-1 endonuclease-dependent retrotranspositional events causing human genetic disease. Human genetics 117 (5):411-427. doi:10.1007/s00439-005-1321-0

Choi SH, Kim YH, Hebisch M, Sliwinski C, Lee S, D'Avanzo C, Chen H, Hooli B, Asselin C, Muffat J, Klee JB, Zhang C, Wainger BJ, Peitz M, Kovacs DM, Woolf CJ, Wagner SL, Tanzi RE, Kim DY (2014) A three-dimensional human neural cell culture model of Alzheimer's disease. Nature 515 (7526):274-278. doi:10.1038/nature13800

Cordaux R, Batzer MA (2009) The impact of retrotransposons on human genome evolution. Nature reviews Genetics 10 (10):691-703. doi:10.1038/nrg2640

Cost GJ, Feng Q, Jacquier A, Boeke JD (2002) Human L1 element target-primed reverse transcription in vitro. The EMBO Journal 21 (21):5899-5910. doi:10.1093/emboj/cdf592

Coufal NG, Garcia-Perez JL, Peng GE, Marchetto MC, Muotri AR, Mu Y, Carson CT, Macia A, Moran JV, Gage FH (2011) Ataxia telangiectasia mutated (ATM) modulates long interspersed element-1 (L1) retrotransposition in human neural stem cells. Proceedings of the National Academy of Sciences of the United States of America 108 (51):20382-20387. doi:10.1073/pnas.1100273108

Coufal NG, Garcia-Perez JL, Peng GE, Yeo GW, Mu Y, Lovci MT, Morell M, O'Shea KS, Moran JV, Gage FH (2009) L1 retrotransposition in human neural progenitor cells. Nature 460 (7259):1127-1131. doi:10.1038/nature08248

Cugola FR, Fernandes IR, Russo FB, Freitas BC, Dias JL, Guimaraes KP, Benazzato C, Almeida N, Pignatari GC, Romero S, Polonio CM, Cunha I, Freitas CL, Brandao WN, Rossato C, Andrade DG, Faria Dde P, Garcez AT, Buchpigel CA, Braconi CT, Mendes E, Sall AA, Zanotto PM, Peron JP, Muotri AR, Beltrao-Braga PC (2016) The Brazilian Zika virus strain causes birth defects in experimental models. Nature 534 (7606):267-271. doi:10.1038/nature18296

Dai L, Huang Q, Boeke JD (2011) Effect of reverse transcriptase inhibitors on LINE-1 and Ty1 reverse transcriptase activities and on LINE-1 retrotransposition. BMC Biochemistry 12 (1):18. doi:10.1186/1471-2091-12-18

Denli AM, Narvaiza I, Kerman BE, Pena M, Benner C, Marchetto MC, Diedrich JK, Aslanian A, Ma J, Moresco JJ, Moore L, Hunter T, Saghatelian A, Gage FH (2015) Primate-specific ORF0 contributes to retrotransposon-mediated diversity. Cell 163 (3):583-593. doi:10.1016/j.cell.2015.09.025

Dmitriev SE, Andreev DE, Terenin IM, Olovnikov IA, Prassolov VS, Merrick WC, Shatsky IN (2007) Efficient translation initiation directed by the 900-nucleotide-long and GC-rich 5' untranslated region of the human retrotransposon LINE-1 mRNA is strictly cap dependent rather than internal ribosome entry site mediated. Molecular and Cellular Biology 27 (13):4685-4697. doi:10.1128/mcb.02138-06

Dombroski BA, Mathias SL, Nanthakumar E, Scott AF, Kazazian HH, Jr. (1991) Isolation of an active human transposable element. Science (New York, NY) 254 (5039):1805-1808

Doucet AJ, Hulme AE, Sahinovic E, Kulpa DA, Moldovan JB, Kopera HC, Athanikar JN, Hasnaoui M, Bucheton A, Moran JV, Gilbert N (2010) Characterization of LINE-1 ribonucleoprotein particles. PLoS genetics 6 (10). doi:10.1371/journal.pgen.1001150

Doyle GA, Crist RC, Karatas ET, Hammond MJ, Ewing AD, Ferraro TN, Hahn CG, Berrettini WH (2017) Analysis of LINE-1 Elements in DNA from Postmortem Brains of Individuals with Schizophrenia. Neuropsychopharmacology : official publication of the American College of Neuropsychopharmacology. doi:10.1038/npp.2017.115

Evrony GD (2015) Cell lineage analysis in human brain using endogenous. 85 (1):49-59. doi:10.1016/j.neuron.2014.12.028

Evrony GD, Cai X, Lee E, Hills LB, Elhosary PC, Lehmann HS, Parker JJ, Atabay KD, Gilmore EC, Poduri A, Park PJ, Walsh CA (2012) Single-neuron sequencing analysis of L1 retrotransposition and somatic mutation in the human brain. Cell 151 (3):483-496. doi:10.1016/j.cell.2012.09.035

Feng Q, Moran JV, Kazazian HH, Jr., Boeke JD (1996) Human L1 retrotransposon encodes a conserved endonuclease required for retrotransposition. Cell 87 (5):905-916

Garcez PP, Loiola EC, Madeiro da Costa R, Higa LM, Trindade P, Delvecchio R, Nascimento JM, Brindeiro R, Tanuri A, Rehen SK (2016) Zika virus impairs growth in human neurospheres and brain organoids. Science (New York, NY)

Garcia Perez JL, Alarcon-Riquelme ME (2017) The TREX1 Dinosaur Bites the Brain through the LINE. Cell stem cell 21 (3):287-288. doi:10.1016/j.stem.2017.08.010

Garcia-Perez JL, Marchetto MC, Muotri AR, Coufal NG, Gage FH, O'Shea KS, Moran JV (2007) LINE-1 retrotransposition in human embryonic stem cells. Human molecular genetics 16 (13):1569-1577. doi:10.1093/hmg/ddm105

Garcia-Perez JL, Morell M, Scheys JO, Kulpa DA, Morell S, Carter CC, Hammer GD, Collins KL, O'Shea KS, Menendez P, Moran JV (2010) Epigenetic silencing of engineered L1 retrotransposition events in human embryonic carcinoma cells. Nature 466 (7307):769-773. doi:10.1038/nature09209

Goodier JL (2014) Retrotransposition in tumors and brains. Mobile DNA 5 (1):11. doi:10.1186/1759-8753-5-11

Goodier JL, Zhang L, Vetter MR, Kazazian HH, Jr. (2007) LINE-1 ORF1 protein localizes in stress granules with other RNA-binding proteins, including components of RNA interference RNA-induced silencing complex. Molecular and Cellular Biology 27 (18):6469-6483. doi:10.1128/mcb.00332-07

Guastella AJ, Richardson R, Lovibond PF, Rapee RM, Gaston JE, Mitchell P, Dadds MR (2008) A randomized controlled trial of D-cycloserine enhancement of exposure therapy for social anxiety disorder. Biological psychiatry 63 (6):544-549

Guffanti G, Gaudi S, Klengel T, Fallon JH, Mangalam H, Madduri R, Rodriguez A, DeCrescenzo P, Glovienka E, Sobell J, Klengel C, Pato M, Ressler KJ, Pato C, Macciardi F (2016) LINE1 insertions as a genomic risk factor for schizophrenia: Preliminary evidence from an affected family. American journal of medical genetics Part B, Neuropsychiatric genetics : the official publication of the International Society of Psychiatric Genetics 171 (4):534-545. doi:10.1002/ajmg.b.32437

Hagberg B, Aicardi J, Dias K, Ramos O (1983) A progressive syndrome of autism, dementia, ataxia, and loss of purposeful hand use in girls: Rett's syndrome: report of 35 cases. Annals of neurology 14 (4):471-479

Hagberg B, Anvret M, Wahlström J (1993) Rett Syndrome-Clinical and Biological Aspects: Studies on 130 Swedish Females. vol 127. Cambridge University Press

Hagberg B, Goutières F, Hanefeld F, Rett A, Wilson J (1985) Rett syndrome: criteria for inclusion and exclusion. Brain and Development 7 (3):372-373

Hagberg BA, Skjeldal OH (1994) Rett variants: a suggested model for inclusion criteria. Pediatric neurology 11 (1):5-11

Hammer S, Dorrani N, Dragich J, Kudo S, Schanen C (2002) The phenotypic consequences of MECP2 mutations extend beyond Rett syndrome. Mental retardation and developmental disabilities research reviews 8 (2):94-98. doi:10.1002/mrdd.10023

Heras SR, Macias S, Caceres JF, Garcia-Perez JL (2014) Control of mammalian retrotransposons by cellular RNA processing activities. Mobile genetic elements 4:e28439. doi:10.4161/mge.28439

Heras SR, Macias S, Plass M, Fernandez N, Cano D, Eyras E, Garcia-Perez JL, Caceres JF (2013) The Microprocessor controls the activity of mammalian retrotransposons. Nature structural & molecular biology 20 (10):1173-1181. doi:10.1038/nsmb.2658

Hofmann SG, Meuret AE, Smits JA, Simon NM, Pollack MH, Eisenmenger K, Shiekh M, Otto MW (2006) Augmentation of exposure therapy with D-cycloserine for social anxiety disorder. Archives of general psychiatry 63 (3):298-304

Hohjoh H, Singer MF (1997a) Ribonuclease and high salt sensitivity of the ribonucleoprotein complex formed by the human LINE-1 retrotransposon. Journal of molecular biology 271 (1):7-12. doi:10.1006/jmbi.1997.1159

Hohjoh H, Singer MF (1997b) Sequence-specific single-strand RNA binding protein encoded by the human LINE-1 retrotransposon. The EMBO Journal 16 (19):6034-6043. doi:10.1093/emboj/16.19.6034

Holmes SE, Dombroski BA, Krebs CM, Boehm CD, Kazazian HH, Jr. (1994) A new retrotransposable human L1 element from the LRE2 locus on chromosome 1q produces a chimaeric insertion. Nature genetics 7 (2):143-148. doi:10.1038/ng0694-143

Iefremova V, Manikakis G, Krefft O, Jabali A, Weynans K, Wilkens R, Marsoner F, Brandl B, Muller FJ, Koch P, Ladewig J (2017) An Organoid-Based Model of Cortical Development Identifies Non-Cell-Autonomous Defects in Wnt Signaling Contributing to Miller-Dieker Syndrome. Cell reports 19 (1):50-59. doi:10.1016/j.celrep.2017.03.047

Jones RB, Garrison KE, Wong JC, Duan EH, Nixon DF, Ostrowski MA (2008) Nucleoside Analogue Reverse Transcriptase Inhibitors Differentially Inhibit Human LINE-1 Retrotransposition. PLoS ONE 3 (2):e1547. doi:10.1371/journal.pone.0001547

Jurka J (1997) Sequence patterns indicate an enzymatic involvement in integration of mammalian retroposons. Proceedings of the National Academy of Sciences 94 (5):1872-1877

Kang X, Xu H, Teng S, Zhang X, Deng Z, Zhou L, Zuo P, Liu B, Liu B, Wu Q, Wang L, Hu M, Dou H, Liu W, Zhu F, Li Q, Guo S, Gu J, Lei Q, Lu J, Mu Y, Jin M, Wang S, Jiang W, Liu K, Wang C, Li W, Zhang K, Zhou Z (2014) Dopamine release from transplanted neural stem cells in Parkinsonian rat striatum in vivo. Proceedings of the National Academy of Sciences of the United States of America 111 (44):15804-15809. doi:10.1073/pnas.1408484111

Kazazian HH, Jr., Moran JV (2017) Mobile DNA in Health and Disease. The New England journal of medicine 377 (4):361-370. doi:10.1056/NEJMra1510092

Kazazian HH, Jr., Wong C, Youssoufian H, Scott AF, Phillips DG, Antonarakis SE (1988) Haemophilia A resulting from de novo insertion of L1 sequences represents a novel mechanism for mutation in man. Nature 332 (6160):164-166. doi:10.1038/332164a0

Khazina E, Weichenrieder O (2009) Non-LTR retrotransposons encode noncanonical RRM domains in their first open reading frame. Proceedings of the National Academy of Sciences 106 (3):731-736. doi:10.1073/pnas.0809964106

Kishi N, Macklis JD (2004) MECP2 is progressively expressed in post-migratory neurons and is involved in neuronal maturation rather than cell fate decisions. Molecular and cellular neurosciences 27 (3):306-321. doi:10.1016/j.mcn.2004.07.006

Klose RJ, Sarraf SA, Schmiedeberg L, McDermott SM, Stancheva I, Bird AP (2005) DNA binding selectivity of MeCP2 due to a requirement for A/T sequences adjacent to methyl-CpG. Molecular cell 19 (5):667-678. doi:10.1016/j.molcel.2005.07.021

Krishnan N, Krishnan K, Connors CR, Choy MS, Page R, Peti W, Van Aelst L, Shea SD, Tonks NK (2015) PTP1B inhibition suggests a therapeutic strategy for Rett syndrome. The Journal of clinical investigation 125 (8):3163-3177. doi:10.1172/jci80323

Kulpa DA, Moran JV (2005) Ribonucleoprotein particle formation is necessary but not sufficient for LINE-1 retrotransposition. Human molecular genetics 14 (21):3237-3248. doi:10.1093/hmg/ddi354

Kushner MG, Kim SW, Donahue C, Thuras P, Adson D, Kotlyar M, McCabe J, Peterson J, Foa EB (2007) D-cycloserine augmented exposure therapy for obsessive-compulsive disorder. Biological psychiatry 62 (8):835-838

Lancaster MA, Renner M, Martin C-A, Wenzel D, Bicknell LS, Hurles ME, Homfray T, Penninger JM, Jackson AP, Knoblich JA (2013) Cerebral organoids model human brain development and microcephaly. Nature 501:373. doi:10.1038/nature12517 https://www.nature.com/articles/nature12517 - supplementary-information

Lander ES, Linton LM, Birren B, Nusbaum C, Zody MC, Baldwin J, Devon K, Dewar K, Doyle M, FitzHugh W, Funke R, Gage D, Harris K, Heaford A, Howland J, Kann L, Lehoczky J, LeVine R, McEwan P, McKernan K, Meldrim J, Mesirov JP, Miranda C, Morris W,

Naylor J, Raymond C, Rosetti M, Santos R, Sheridan A, Sougnez C, Stange-Thomann Y, Stojanovic N, Subramanian A, Wyman D, Rogers J, Sulston J, Ainscough R, Beck S, Bentley D, Burton J, Clee C, Carter N, Coulson A, Deadman R, Deloukas P, Dunham A, Dunham I, Durbin R, French L, Grafham D, Gregory S, Hubbard T, Humphray S, Hunt A, Jones M, Lloyd C, McMurray A, Matthews L, Mercer S, Milne S, Mullikin JC, Mungall A, Plumb R, Ross M, Shownkeen R, Sims S, Waterston RH, Wilson RK, Hillier LW, McPherson JD, Marra MA, Mardis ER, Fulton LA, Chinwalla AT, Pepin KH, Gish WR, Chissoe SL, Wendl MC, Delehaunty KD, Miner TL, Delehaunty A, Kramer JB, Cook LL, Fulton RS, Johnson DL, Minx PJ, Clifton SW, Hawkins T, Branscomb E, Predki P, Richardson P, Wenning S, Slezak T, Doggett N, Cheng JF, Olsen A, Lucas S, Elkin C, Uberbacher E, Frazier M, Gibbs RA, Muzny DM, Scherer SE, Bouck JB, Sodergren EJ, Worley KC, Rives CM, Gorrell JH, Metzker ML, Naylor SL, Kucherlapati RS, Nelson DL, Weinstock GM, Sakaki Y, Fujiyama A, Hattori M, Yada T, Toyoda A, Itoh T, Kawagoe C, Watanabe H, Totoki Y, Taylor T, Weissenbach J, Heilig R, Saurin W, Artiguenave F, Brottier P, Bruls T, Pelletier E, Robert C, Wincker P, Smith DR, Doucette-Stamm L, Rubenfield M, Weinstock K, Lee HM, Dubois J, Rosenthal A, Platzer M, Nyakatura G, Taudien S, Rump A, Yang H, Yu J, Wang J, Huang G, Gu J, Hood L, Rowen L, Madan A, Qin S, Davis RW, Federspiel NA, Abola AP, Proctor MJ, Myers RM, Schmutz J, Dickson M, Grimwood J, Cox DR, Olson MV, Kaul R, Raymond C, Shimizu N, Kawasaki K, Minoshima S, Evans GA, Athanasiou M, Schultz R, Roe BA, Chen F, Pan H, Ramser J, Lehrach H, Reinhardt R, McCombie WR, de la Bastide M, Dedhia N, Blocker H, Hornischer K, Nordsiek G, Agarwala R, Aravind L, Bailey JA, Bateman A, Batzoglou S, Birney E, Bork P, Brown DG, Burge CB, Cerutti L, Chen HC, Church D, Clamp M, Copley RR, Doerks T, Eddy SR, Eichler EE, Furey TS, Galagan J, Gilbert JG, Harmon C, Hayashizaki Y, Haussler D, Hermjakob H, Hokamp K, Jang W, Johnson LS, Jones TA, Kasif S, Kaspryzk A, Kennedy S, Kent WJ, Kitts P, Koonin EV, Korf I, Kulp D, Lancet D, Lowe TM, McLysaght A, Mikkelsen T, Moran JV, Mulder N, Pollara VJ, Ponting CP, Schuler G, Schultz J, Slater G, Smit AF, Stupka E, Szustakowki J, Thierry-Mieg D, Thierry-Mieg J, Wagner L, Wallis J, Wheeler R, Williams A, Wolf YI, Wolfe KH, Yang SP, Yeh RF, Collins F, Guyer MS, Peterson J, Felsenfeld A, Wetterstrand KA, Patrinos A, Morgan MJ, de Jong P, Catanese JJ, Osoegawa K, Shizuya H, Choi S, Chen YJ, Szustakowki J (2001) Initial sequencing and analysis of the human genome. Nature 409 (6822):860-921. doi:10.1038/35057062

Luan DD, Korman MH, Jakubczak JL, Eickbush TH (1993) Reverse transcription of R2Bm RNA is primed by a nick at the chromosomal target site: a mechanism for non-LTR retrotransposition. Cell 72 (4):595-605

MacLennan M, Garcia-Canadas M, Reichmann J, Khazina E, Wagner G, Playfoot CJ, Salvador-Palomeque C, Mann AR, Peressini P, Sanchez L, Dobie K, Read D, Hung CC, Eskeland R, Meehan RR, Weichenrieder O, Garcia-Perez JL, Adams IR (2017) Mobilization of LINE-1 retrotransposons is restricted by Tex19.1 in mouse embryonic stem cells. eLife 6. doi:10.7554/eLife.26152

Marchetto MC, Carromeu C, Acab A, Yu D, Yeo GW, Mu Y, Chen G, Gage FH, Muotri AR (2010) A model for neural development and treatment of Rett syndrome using human induced pluripotent stem cells. Cell 143 (4):527-539. doi:10.1016/j.cell.2010.10.016

Marchetto MCN, Narvaiza I, Denli AM, Benner C, Lazzarini TA, Nathanson JL, Paquola ACM, Desai KN, Herai RH, Weitzman MD, Yeo GW, Muotri AR, Gage FH (2013) Differential L1 regulation in pluripotent stem cells of humans and apes. Nature 503 (7477):525-529. doi:10.1038/nature12686

Mariani J, Coppola G, Zhang P, Abyzov A, Provini L, Tomasini L, Amenduni M, Szekely A, Palejev D, Wilson M, Gerstein M, Grigorenko EL, Chawarska K, Pelphrey KA, Howe JR, Vaccarino FM (2015) FOXG1-Dependent Dysregulation of GABA/Glutamate Neuron Differentiation in Autism Spectrum Disorders. Cell 162 (2):375-390. doi:10.1016/j.cell.2015.06.034

Martin F, Maranon C, Olivares M, Alonso C, Lopez MC (1995) Characterization of a non-long terminal repeat retrotransposon cDNA (L1Tc) from Trypanosoma cruzi: homology of the first ORF with the ape family of DNA repair enzymes. Journal of molecular biology 247 (1):49-59. doi:10.1006/jmbi.1994.0121

Martin SL (1991) Ribonucleoprotein particles with LINE-1 RNA in mouse embryonal carcinoma cells. Molecular and Cellular Biology 11 (9):4804-4807. doi:10.1128/mcb.11.9.4804

Martin SL, Bushman FD (2001) Nucleic acid chaperone activity of the ORF1 protein from the mouse LINE-1 retrotransposon. Molecular and Cellular Biology 21 (2):467-475. doi:10.1128/mcb.21.2.467-475.2001

Mathias SL, Scott AF, Kazazian HH, Jr., Boeke JD, Gabriel A (1991) Reverse transcriptase encoded by a human transposable element. Science (New York, NY) 254 (5039):1808-1810

Mills RE, Bennett EA, Iskow RC, Devine SE (2007) Which transposable elements are active in the human genome? Trends in genetics : TIG 23 (4):183-191. doi:10.1016/j.tig.2007.02.006

Monot C, Kuciak M, Viollet S, Mir AA, Gabus C, Darlix JL, Cristofari G (2013) The specificity and flexibility of l1 reverse transcription priming at imperfect T-tracts. PLoS genetics 9 (5):e1003499. doi:10.1371/journal.pgen.1003499

Moran JV, Gilbert N (2002) Mammalian LINE-1 retrotransposons and related elements. In: Mobile DNA II. American Society of Microbiology, pp 836-869

Moran JV, Holmes SE, Naas TP, DeBerardinis RJ, Boeke JD, Kazazian HH, Jr. (1996) High frequency retrotransposition in cultured mammalian cells. Cell 87 (5):917-927

Munoz-Lopez M, Macia A, Garcia-Canadas M, Badge RM, Garcia-Perez JL (2011) An epi [c] genetic battle: LINE-1 retrotransposons and intragenomic conflict in humans. Mobile genetic elements 1 (2):122-127. doi:10.4161/mge.1.2.16730

Muotri AR, Chu VT, Marchetto MCN, Deng W, Moran JV, Gage FH (2005) Somatic mosaicism in neuronal precursor cells mediated by L1 retrotransposition. Nature 435. doi:10.1038/nature03663

Muotri AR, Marchetto MC, Coufal NG, Oefner R, Yeo G, Nakashima K, Gage FH (2010) L1 retrotransposition in neurons is modulated by MeCP2. Nature 468 (7322):443-446. doi:10.1038/nature09544

Na ES, De Jesús-Cortés H, Martinez-Rivera A, Kabir ZD, Wang J, Ramesh V, Onder Y, Rajadhyaksha AM, Monteggia LM, Pieper AA (2017) D-cycloserine improves synaptic transmission in an animal mode of Rett syndrome. PLoS ONE 12 (8):e0183026. doi:10.1371/journal.pone.0183026

Nageshappa S, Carromeu C, Trujillo CA, Mesci P, Espuny-Camacho I, Pasciuto E, Vanderhaeghen P, Verfaillie CM, Raitano S, Kumar A, Carvalho CM, Bagni C, Ramocki MB, Araujo BH, Torres LB, Lupski JR, Van Esch H, Muotri AR (2016) Altered neuronal network and rescue in a human MECP2 duplication model. Molecular psychiatry 21 (2):178-188. doi:10.1038/mp.2015.128

Newkirk SJ, Lee S, Grandi FC, Gaysinskaya V, Rosser JM, Vanden Berg N, Hogarth CA, Marchetto MCN, Muotri AR, Griswold MD, Ye P, Bortvin A, Gage FH, Boeke JD, An W (2017) Intact piRNA pathway prevents L1 mobilization in male meiosis. Proceedings of the National Academy of Sciences of the United States of America 114 (28):E5635-e5644. doi:10.1073/pnas.1701069114

Ostertag EM, Luning Prak ET, DeBerardinis RJ, Moran JV (2000) Determination of L1 retrotransposition kinetics in cultured cells. 28 (6):1418-1423

Otto MW, Tolin DF, Simon NM, Pearlson GD, Basden S, Meunier SA, Hofmann SG, Eisenmenger K, Krystal JH, Pollack MH (2010) Efficacy of d-cycloserine for enhancing response to cognitive-behavior therapy for panic disorder. Biological psychiatry 67 (4):365-370

Pasca AM, Sloan SA, Clarke LE, Tian Y, Makinson CD, Huber N, Kim CH, Park JY, O'Rourke NA, Nguyen KD, Smith SJ, Huguenard JR, Geschwind DH, Barres BA, Pasca SP (2015) Functional cortical neurons and astrocytes from human pluripotent stem cells in 3D culture. Nature methods 12 (7):671-678. doi:10.1038/nmeth.3415

Perepelitsa-Belancio V, Deininger P (2003) RNA truncation by premature polyadenylation attenuates human mobile element activity. Nature genetics 35 (4):363-366. doi:10.1038/ng1269

Ressler KJ, Rothbaum BO, Tannenbaum L, Anderson P, Graap K, Zimand E, Hodges L, Davis M (2004) Cognitive enhancers as adjuncts to psychotherapy: Use of D-cycloserine in phobic individuals to facilitate extinctionof fear. Archives of general psychiatry 61 (11):1136-1144

Richardson SR, Narvaiza I, Planegger RA, Weitzman MD, Moran JV (2014) APOBEC3A deaminates transiently exposed single-strand DNA during LINE-1 retrotransposition. eLife 3:e02008. doi:10.7554/eLife.02008

Samaco RC, Hogart A, LaSalle JM (2005) Epigenetic overlap in autism-spectrum neurodevelopmental disorders: MECP2 deficiency causes reduced expression of UBE3A and GABRB3. Human molecular genetics 14 (4):483-492. doi:10.1093/hmg/ddi045

Samaco RC, Nagarajan RP, Braunschweig D, LaSalle JM (2004) Multiple pathways regulate MeCP2 expression in normal brain development and exhibit defects in autism-spectrum disorders. Human molecular genetics 13 (6):629-639. doi:10.1093/hmg/ddh063

Schollen E, Smeets E, Deflem E, Fryns JP, Matthijs G (2003) Gross rearrangements in the MECP2 gene in three patients with Rett syndrome: implications for routine diagnosis of Rett syndrome. Human mutation 22 (2):116-120. doi:10.1002/humu.10242

Schumann GG (2007) APOBEC3 proteins: major players in intracellular defence against LINE-1-mediated retrotransposition. Biochemical Society transactions 35 (Pt 3):637-642. doi:10.1042/bst0350637

Schwahn U, Lenzner S, Dong J, Feil S, Hinzmann B, van Duijnhoven G, Kirschner R, Hemberger M, Bergen AA, Rosenberg T, Pinckers AJ, Fundele R, Rosenthal A, Cremers FP, Ropers HH, Berger W (1998) Positional cloning of the gene for X-linked retinitis pigmentosa 2. Nature genetics 19 (4):327-332. doi:10.1038/1214

Scott AF, Schmeckpeper BJ, Abdelrazik M, Comey CT, O'Hara B, Rossiter JP, Cooley T, Heath P, Smith KD, Margolet L (1987) Origin of the human L1 elements: proposed progenitor genes deduced from a consensus DNA sequence. Genomics 1 (2):113-125

Sheinin A, Shavit S, Benveniste M (2001) Subunit specificity and mechanism of action of NMDA partial agonist D-cycloserine. Neuropharmacology 41 (2):151-158

Shen Y, Chow J, Wang Z, Fan G (2006) Abnormal CpG island methylation occurs during in vitro differentiation of human embryonic stem cells. Human molecular genetics 15 (17):2623-2635. doi:10.1093/hmg/ddl188

Sokolowski M, Chynces M, deHaro D, Christian CM, Belancio VP (2017) Truncated ORF1 proteins can suppress LINE-1 retrotransposition in trans. Nucleic acids research 45 (9):5294-5308. doi:10.1093/nar/gkx211

Speek M (2001) Antisense Promoter of Human L1 Retrotransposon Drives Transcription of Adjacent Cellular Genes. Molecular and Cellular Biology 21 (6):1973-1985. doi:10.1128/mcb.21.6.1973-1985.2001

Takahashi K, Tanabe K, Ohnuki M, Narita M, Ichisaka T, Tomoda K, Yamanaka S (2007) Induction of pluripotent stem cells from adult human fibroblasts by defined factors. Cell 131 (5):861-872. doi:10.1016/j.cell.2007.11.019

Takahashi K, Yamanaka S (2006) Induction of pluripotent stem cells from mouse embryonic and adult fibroblast cultures by defined factors. Cell 126 (4):663-676. doi:10.1016/j.cell.2006.07.024

Tang X, Kim J, Zhou L, Wengert E, Zhang L, Wu Z, Carromeu C, Muotri AR, Marchetto MCN, Gage FH, Chen G (2016) KCC2 rescues functional deficits in human neurons derived from patients with Rett syndrome. Proceedings of the National Academy of Sciences of the United States of America 113 (3):751-756. doi:10.1073/pnas.1524013113

Telesnitsky A, Goff SP (1997) Reverse Transcriptase and the Generation of Retroviral DNA. In: Coffin JM, Hughes SH, Varmus HE (eds) Retroviruses. Cold Spring Harbor Laboratory Press. Cold Spring Harbor Laboratory Press., Cold Spring Harbor (NY),

Thayer RE, Singer MF, Fanning TG (1993) Undermethylation of specific LINE-1 sequences in human cells producing a LINE-1-encoded protein. Gene 133 (2):273-277

Thomas CA, Tejwani L, Trujillo CA, Negraes PD, Herai RH, Mesci P, Macia A, Crow YJ, Muotri AR (2017) Modeling of TREX1-Dependent Autoimmune Disease using Human Stem Cells Highlights L1 Accumulation as a Source of Neuroinflammation. Cell stem cell. doi:10.1016/j.stem.2017.07.009

Thomson JA, Itskovitz-Eldor J, Shapiro SS, Waknitz MA, Swiergiel JJ, Marshall VS, Jones JM (1998) Embryonic stem cell lines derived from human blastocysts. Science (New York, NY) 282 (5391):1145-1147

Tropea D, Giacometti E, Wilson NR, Beard C, McCurry C, Fu DD, Flannery R, Jaenisch R, Sur M (2009) Partial reversal of Rett Syndrome-like symptoms in MeCP2 mutant mice. Proceedings of the National Academy of Sciences of the United States of America 106 (6):2029-2034. doi:10.1073/pnas.0812394106

Upton KR, Gerhardt DJ, Jesuadian JS, Richardson SR, Sanchez-Luque FJ, Bodea GO, Ewing AD, Salvador-Palomeque C, van der Knaap MS, Brennan PM, Vanderver A, Faulkner GJ (2015) Ubiquitous L1 mosaicism in hippocampal neurons. Cell 161 (2):228-239. doi:10.1016/j.cell.2015.03.026

Wei W, Gilbert N, Ooi SL, Lawler JF, Ostertag EM, Kazazian HH, Boeke JD, Moran JV (2001) Human L1 retrotransposition: cis preference versus trans complementation. Molecular and Cellular Biology 21 (4):1429-1439. doi:10.1128/mcb.21.4.1429-1439.2001

Wilhelm S, Buhlmann U, Tolin DF, Meunier SA, Pearlson GD, Reese HE, Cannistraro P, Jenike MA, Rauch SL (2008) Augmentation of behavior therapy with D-cycloserine for obsessive-compulsive disorder. American journal of psychiatry 165 (3):335-341

Wissing S, Montano M, Garcia-Perez JL, Moran JV, Greene WC (2011) Endogenous APOBEC3B restricts LINE-1 retrotransposition in transformed cells and human embryonic stem cells. The Journal of biological chemistry 286 (42):36427-36437. doi:10.1074/jbc.M111.251058

Wissing S, Munoz-Lopez M, Macia A, Yang Z, Montano M, Collins W, Garcia-Perez JL, Moran JV, Greene WC (2012) Reprogramming somatic cells into iPS cells activates LINE-1 retroelement mobility. Human molecular genetics 21 (1):208-218. doi:10.1093/hmg/ddr455

Xiol J, Spinelli P, Laussmann Maike A, Homolka D, Yang Z, Cora E, Couté Y, Conn S, Kadlec J, Sachidanandam R, Kaksonen M, Cusack S, Ephrussi A, Pillai Ramesh S (2014) RNA Clamping by Vasa Assembles a piRNA Amplifier Complex on Transposon Transcripts. Cell 157 (7):1698-1711. doi:10.1016/j.cell.2014.05.018

Yang N, Kazazian HH, Jr. (2006) L1 retrotransposition is suppressed by endogenously encoded small interfering RNAs in human cultured cells. Nature structural & molecular biology 13 (9):763-771. doi:10.1038/nsmb1141

Yasui DH, Peddada S, Bieda MC, Vallero RO, Hogart A, Nagarajan RP, Thatcher KN, Farnham PJ, Lasalle JM (2007) Integrated epigenomic analyses of neuronal MeCP2 reveal a role for long-range interaction with active genes. Proceedings of the National Academy of Sciences of the United States of America 104 (49):19416-19421. doi:10.1073/pnas.0707442104

Yu F, Zingler N, Schumann G, Stratling WH (2001) Methyl-CpG-binding protein 2 represses LINE-1 expression and retrotransposition but not Alu transcription. Nucleic acids research 29 (21):4493-4501

Zappella M, Meloni I, Longo I, Canitano R, Hayek G, Rosaia L, Mari F, Renieri A (2003) Study of MECP2 gene in Rett syndrome variants and autistic girls. American journal of medical genetics Part B, Neuropsychiatric genetics : the official publication of the International Society of Psychiatric Genetics 119b (1):102-107. doi:10.1002/ajmg.b.10070

Zhang A, Dong B, Doucet AJ, Moldovan JB, Moran JV, Silverman RH (2014) RNase L restricts the mobility of engineered retrotransposons in cultured human cells. Nucleic acids research 42 (6):3803-3820. doi:10.1093/nar/gkt1308